RM No. L8H31

NACA

RESEARCH MEMORANDUM

AN INVESTIGATION OF THE LOW-SPEED STATIC STABILITY CHARACTERISTICS OF COMPLETE MODELS HAVING SWEPTBACK AND SWEPTFORWARD WINGS

By

M. Leroy Spearman and Paul Comisarow

Langley Aeronautical Laboratory
Langley Field, Va.

NATIONAL ADVISORY COMMITTEE FOR AERONAUTICS

WASHINGTON
November 19, 1948

NACA RM No. L8H31 RESTRICTED

NATIONAL ADVISORY COMMITTEE FOR AERONAUTICS

RESEARCH MEMORANDUM

AN INVESTIGATION OF THE LOW-SPEED STATIC STABILITY CHARACTERISTICS OF COMPLETE MODELS HAVING SWEPTBACK AND SWEPTFORWARD WINGS

By M. Leroy Spearman and Paul Comisarow

SUMMARY

An investigation has been conducted in the Langley 300 MPH 7- by 10-foot tunnel to determine the static stability characteristics at low speeds of complete models with various swept wings so that comparisons might be made with available theoretical and empirical methods of predicting the stability characteristics. Longitudinal and lateral stability characteristics, flaps up and down, were obtained for models having 0°, 15°, 30°, and 45° sweptforward and sweptback wings.

The results of the investigation indicate that static stability characteristics can be estimated with reasonable accuracy in the low-lift range by means of existing theories.

For lift coefficients near the stall where no theory is applicable, the longitudinal-stability trends for the complete models were similar to those that might be expected from an inspection of isolated swept-wing data.

INTRODUCTION

Experimental and theoretical investigations have shown that the use of wings having large angles of sweep might introduce serious low-speed stability problems. The results of an investigation reported in reference 1 on the stability characteristics of small-scale sweptback and sweptforward wings and in reference 2 for large-scale sweptback and sweptforward wings indicate that fairly accurate estimates can be made of the characteristics of isolated swept wings at low and moderate lift coefficients before separation effects assume any importance.

It was not certain, however, that the characteristics of complete models with swept wings could be predicted with as high a degree of accuracy as those of the isolated wing. Heretofore no systematic investigation of complete models with various sweptback and sweptforward wings has been made. The purpose of the present paper is to present

the results of such an investigation made to determine the longitudinal and lateral stability characteristics of models with various sweptback and sweptforward wings and to show comparisons with available theoretical and empirical results.

COEFFICIENTS AND SYMBOLS

The results of the tests are presented as standard NACA coefficients of forces and moments. All forces and moments are presented for the stability axes shown in figure 1 with the reference center of gravity at the 25 percent mean aerodynamic chord for each model as indicated in figure 2.

The coefficients and symbols are defined as follows:

C_L	lift coefficient (Lift/qS where Lift = -Z)
ΔC_L	increment of lift coefficient due to flap deflection
C_X	longitudinal-force coefficient (X/qS)
C_Y	lateral-force coefficient (Y/qS)
C_l	rolling-moment coefficient (L/qSb)
C_m	pitching-moment coefficient (M/qS$\bar{c}$)
C_n	yawing-moment coefficient (N/qSb)
Z	force along Z-axis, pounds
X	force along X-axis, pounds
Y	force along Y-axis, pounds
L	rolling moment about X-axis, pound-feet
M	pitching moment about Y-axis, pound-feet
N	yawing moment about Z-axis, pound-feet
q	free-stream dynamic pressure, pounds per square foot ($\rho V^2/2$)
S	wing area, square feet
b	wing span, feet

$\bar{c}$	wing mean aerodynamic chord, feet $\left(\frac{2}{S}\int_0^{b/2} c^2\, dy\right)$
ρ	mass density of air, slug per cubic foot
V	air velocity, feet per second
c	airfoil section chord, feet
y	distance along wing span, feet
A	aspect ratio (b^2/S)
Λ	angle of sweep of wing quarter-chord line, degrees (positive for sweepback)
λ	taper ratio $\left(\frac{\text{Tip chord}}{\text{Root chord}}\right)$
l_t	tail length measured from center of gravity to the elevator hinge line, feet
α	angle of attack of wing chord line, degrees
ψ	angle of yaw, degrees
ϵ	angle of downwash, degrees
i_t	angle of stabilizer with respect to wing chord line, degrees
δ_f	flap deflection measured perpendicular to 80-percent-chord line, degrees
n_p	neutral-point location, percent wing mean aerodynamic chord
M_o	tunnel free-stream Mach number

Subscripts:

f	denotes sweptforward wing tip at $\Lambda = 0^\circ$
b	denotes sweptback wing tip at $\Lambda = 0^\circ$
t	horizontal tail
v.t.	vertical tail

Symbols used as subscripts denote partial derivatives of coefficients with respect to angle of attack, angle of yaw, and lift coefficient. For example:

$$C_{l_{\psi C_L}} = \frac{\partial}{\partial C_L}\left(\frac{\partial C_l}{\partial \psi}\right)$$

MODEL

The models tested in the present investigation had the same fuselage and tail surfaces. The wings used could be pivoted from an unswept position to angles of sweep of ±15°, ±30°, and ±45°. Two pairs of wing tips were used, one for the sweptback wings and one for the sweptforward wings, so designed as to be parallel with the fuselage center line at ±45° sweep. No attempt was made to hold the area, span, or aspect ratio constant for the various sweep configurations. Drawings of the models giving pertinent information are presented in figure 2 and the physical characteristics of the models are given in table I. The span for each model was measured to the extreme tips of the wing. Half-span split flaps of 20 percent chord were tested on all models.

Various models mounted in the Langley 300 MPH 7- by 10-foot tunnel are shown in figure 3.

TESTS AND RESULTS

Test Conditions

Tests were made at a dynamic pressure of 33.6 pounds per square foot (M_o = 0.15). The corresponding Reynolds numbers based on the wing mean aerodynamic chord are as follows:

Λ (deg)	M.A.C. (ft)	Reynolds number
-45	1.888	2,020,000
-30	1.460	1,569,000
-15	1.262	1,357,000
0	1.181	1,270,000
15	1.201	1,292,000
30	1.278	1,373,000
45	1.542	1,657,000

The Reynolds number was computed using a turbulence factor of unity. The degree of turbulence of the tunnel is not known quantitatively but is believed to be small because of the high contraction ratio (14:1).

Corrections

Tare corrections were considered negligible and were not applied. Jet-boundary corrections were computed by the method of reference 3 and an unpublished analysis shows this to be applicable for wings up to 45° sweep. Corrections applied were as follows:

$$\alpha = \alpha_M + EC_{L_M}$$

$$C_X = C_{X_M} - FC_{L_M}^2$$

$$C_m = C_{m_M} + GC_{L_M} \quad \text{(for tail on)}$$

where the subscript M denotes measured values.

The E, F, and G values for each sweep angle are given in the following table:

Λ (deg)	E	F	G
-45	1.160	0.0170	0.0377
-30	1.065	.0154	.0312
-15	1.005	.0153	.0258
0_f	.972	.0153	.0212
0_b	.960	.0152	.0209
15	.926	.0139	.0198
30	.886	.0130	.0187
45	.845	.0129	.0175

All forces and moments were corrected for blocking by the method given in reference 4. An increment in longitudinal-force coefficient has been applied to account for the horizontal buoyancy.

Presentation of Results

A table of figures presenting the results is given as follows:

DISCUSSION

In the analysis of the data each model was considered as an individual configuration. Although the primary physical difference between the models is the angle of sweep, there are irregular variations in the wing area, wing span, mean aerodynamic chord, center-of-gravity location, and tail length accompanying the change in sweep. The results obtained, therefore, do not represent the effect of sweep on the stability characteristics but include all those factors varying as a result of changes in sweep. Consequently, the aerodynamic trends indicated apply only for the models tested and for other configurations may be entirely different. The emphasis then should be placed on the extent to which calculated values of the stability characteristics may be made with reasonable accuracy and not upon the quantitative results shown.

Longitudinal Stability

The static longitudinal stability of a jet airplane in power-off flight at subcritical speeds may be expressed as

$$\frac{dC_m}{dC_L} = \left(\frac{\partial C_m}{\partial C_L}\right)_0 - \left|\frac{\partial C_m}{\partial i_t}\right|\left(1 - \frac{\partial \epsilon}{\partial \alpha}\right)\frac{1}{C_{L_\alpha}}$$

where $\left(\frac{\partial C_m}{\partial C_L}\right)_0$ represents the longitudinal stability of the wing-fuselage combination and $\frac{\partial C_m}{\partial i_t}\left(1 - \frac{\partial \epsilon}{\partial \alpha}\right)\frac{1}{C_{L_\alpha}}$ is the contribution of the tail to

the longitudinal stability. Each of the factors affecting the longitudinal stability was estimated and then by use of the equation the static longitudinal stability for each model was calculated. The results are shown and compared with the experimental results in figure 10.

The variation of the lift-curve slope C_{L_α} with sweep was estimated by the method of reference 5. The basic value of C_{L_α} for the unswept-wing model was found by adding C_{L_α} for the plain wing (0.078 as determined from reference 5) to a value of 0.014 for the fuselage and tail as determined from unpublished results of tests of a similar model.

The stabilizer effectiveness was found from the relation

$$\frac{\partial C_m}{\partial i_t} = \left(C_{L_\alpha}\right)_t \frac{l_t}{\bar{c}} \frac{S_t}{S}$$

By the use of reference 6 a value of 0.060 was estimated for $\left(C_{L_\alpha}\right)_t$.

An empirical method presented in reference 7 was used to estimate the variation of the downwash angle with angle of attack $\frac{\partial \epsilon}{\partial \alpha}$ for the various configurations.

The static longitudinal stability of the wing-fuselage combination $\left(\frac{\partial C_m}{\partial C_L}\right)_0$ was determined by use of the method given in reference 8 which accounts for the interference effects of bodies with swept wings. It is shown in reference 8 that a rearward shift of the wing-fuselage aerodynamic center might occur for bodies with sweptback wings because of a loss in lift on the wing center section caused by the presence of the fuselage. This area of reduced lift, being ahead of the reference center-of-gravity position ($0.25\bar{c}$), would produce a negative pitching moment in opposition to the positive moment always produced by the fuselage. For sweptforward wings the reverse is true and a positive pitching moment is produced by the loss of wing lift in addition to the positive moment of the fuselage. Hence, in comparison with the aerodynamic-center shift of bodies with straight wings, the shift will be more forward for bodies with sweptforward wings and less forward for bodies with sweptback wings. For these calculations it was assumed that the aerodynamic center of the plain wing remained unchanged with sweep.

Each of the factors affecting the static longitudinal stability was estimated with reasonable accuracy and good agreement was obtained between the calculated and experimental values of the total longitudinal stability $\frac{dC_m}{dC_L}$ for each model (fig. 10).

The variation of the neutral point with sweep angle in the low-lift range as determined both experimentally and theoretically is shown in figure 11 and indicates that flap deflection has little effect on the longitudinal stability of these models.

Near maximum lift the pitching-moment characteristics of the models were similar to those that might be expected for isolated wings (reference 9) based on the sweep angle and aspect ratio. As pointed out in reference 2, the predictions of reference 9 apply equally as well to sweptforward wings as to sweptback wings. The models with unswept wings and $\pm 15^\circ$ swept wings are stable or marginally stable near the stall. The models with $\pm 30^\circ$ and $\pm 45^\circ$ swept wings indicate instability with the exception of the -45° wing model with flaps retracted (fig. 5(d)) in which case it appears that an angle of attack high enough to effect a partial wing stall was not attained. The instability of the 30° and 45° sweptback-wing models is caused partly by tip stall as evidenced by the tail-off pitching-moment curve (figs. 4(c) and 4(d)) and partly by the rapid increase in the rate of change of downwash at the higher angles of attack (fig. 12) that results from the inboard shift of the lift. The -30° and -45° swept-wing models show no large downwash changes with sweep and instability should result primarily from wing root stall.

When the flaps are deflected the unstable tendencies near the stall are accentuated. For sweptback wings the tip portion of the wing might stall although the flap prevents complete wing stall and the result is a greater nosing-up tendency of the wing. In the case of sweptforward wings the stall over the inboard portion of the wing is more pronounced when the flaps are deflected which also results in a greater nosing-up tendency of the wing.

Lateral and Directional Stability

Effective dihedral.- The effect of sweep on the variation of effective dihedral with lift coefficient $C_{l_{\psi_{C_L}}}$ in the low-lift range as determined from figures 8 and 9 is shown in figure 14. Values for the theoretical curve also shown in figure 14 were obtained by adding $C_{l_{\psi_{C_L}}}$ for the plain wing to the increment of $C_{l_{\psi_{C_L}}}$ contributed

by the tail. For the wing alone $\left(C_{l_\psi C_L}\right)_\Lambda = \left(C_{l_\psi C_L}\right)_{\Lambda=0} + 0.0044 \tan \Lambda$ where $0.0044 \tan \Lambda$ is the effect of sweep on effective dihedral (reference 1). The values of $\left(C_{l_\psi C_L}\right)_{\Lambda=0}$ are for unswept wings having the same aspect ratio as the swept wing and were determined from a correlation of experimental results for various unswept wings of different aspect ratios presented in reference 10.

In order to determine the vertical-tail contribution to $C_{l_\psi C_L}$ the lateral-force parameter for the tail was first estimated from $\left(C_{Y_\psi}\right)_{v.t.} = \left(C_{L_\alpha}\right)_{v.t.} \frac{S_{v.t.}}{S}$. By the method of reference 6, which takes into account the end-plate effect of the horizontal tail, a value of 0.062 was obtained for the vertical-tail lift-curve slope based on an aspect ratio of 2.4. The contribution of the tail to C_{l_ψ} at any angle of attack then is $\left(C_{l_\psi}\right)_{v.t.} = \left(C_{Y_\psi}\right)_{v.t.} \frac{h}{b}$ where h is the distance from the X-axis to the center of pressure of the vertical tail. At zero angle of attack h was estimated from tail-on and tail-off tests of a similar model to be 1.4 feet.

Interference and sidewash effects resulting from the fuselage and wing were neglected in the computations.

The results of the calculations (fig. 14) indicate good agreement with the experimental values of $C_{l_\psi C_L}$. It is apparent from figure 14 that flap deflection had a negligible effect on the effective-dihedral variation with lift.

Directional stability.- An attempt was made to calculate the directional-stability parameter C_{n_ψ} at zero lift for each model and the results are included with the experimental results in figure 15. Using the values previously estimated for $\left(C_{Y_\psi}\right)_{v.t.}$ the yawing moment due to yaw produced by the tail was determined from $\left(C_{n_\psi}\right)_{v.t.} = \left(C_{Y_\psi}\right)_{v.t.} \frac{l_t}{b}$. The tail contributed a negative C_{n_ψ} (stabilizing) that increased negatively both with sweepback and sweepforward. The fuselage produced a positive C_{n_ψ} (destabilizing) that was calculated by the method of reference 11. The unstable moment

variation with yaw of the fuselage became more positive with sweepback or sweepforward. The summation of the estimated values of C_{n_ψ} for the fuselage and tail (fig. 15) indicate fair qualitative agreement with experimental results in that generally the directional-stability parameter C_{n_ψ} decreases from sweepforward to sweepback. The discrepancy apparent at high angles of sweepback might be caused by interference effects of the wing on the pressure distribution over the aft portion of the fuselage. It is obvious from figure 15 that flaps may have a large effect on the directional stability.

The variation of C_{n_ψ} with lift coefficient is similar to that obtained from investigations of isolated swept wings (references 1 and 2).

Lift and Drag Characteristics

Flap effectiveness.- Theoretically the lift increment produced by deflecting the flap is proportional to $\cos^2\Lambda$ but an additional correction should be applied to account for the aspect-ratio changes. Inasmuch as the calculations for the theoretical lift-curve slope account for the aspect ratio, the lift increment resulting from flap deflection may be expressed as

$$\left(\Delta C_L\right)_\Lambda = \left(\Delta C_L\right)_{\Lambda=0} \cos\Lambda \frac{\left(C_{L_\alpha}\right)_\Lambda}{\left(C_{L_\alpha}\right)_{\Lambda=0}}$$

In figure 16 the theoretical predictions are compared with the experimental results for ΔC_L and show reasonably good agreement.

CONCLUSIONS

The results of low-speed tests of models having 0°, 15°, 30°, and 45° sweptforward and sweptback wings indicated the following conclusions:

1. The static longitudinal stability in the low-lift range can be predicted inasmuch as the factors affecting the stability - the lift-curve slope, downwash, stabilizer effectiveness, and wing-fuselage aerodynamic center - can be estimated accurately by means of existing theories.

2. The variation of effective dihedral with lift coefficient can also be estimated with good accuracy.

3. Predictions of the directional stability can be made with fair accuracy.

4. The increment of lift caused by flap deflection can be estimated with reasonable accuracy.

5. For lift coefficients near the stall where no theories are applicable, the longitudinal stability characteristics for the complete models were similar to those indicated by investigations of isolated swept-wing configurations.

Langley Aeronautical Laboratory
National Advisory Committee for Aeronautics
Langley Field, Va.

REFERENCES

1. Purser, Paul E., and Spearman, M. Leroy: Wind-Tunnel Tests at Low Speed of Swept and Yawed Wings Having Various Plan Forms. NACA RM No. L7D23, 1947.

2. McCormack, Gerald M., and Stevens, Victor I., Jr.: An Investigation of the Low-Speed Stability and Control Characteristics of Swept-Forward and Swept-Back Wings in the Ames 40- by 80-Foot Wind Tunnel. NACA RM No. A6K15, 1947.

3. Gillis, Clarence L., Polhamus, Edward C., and Gray, Joseph L., Jr.: Charts for Determining Jet-Boundary Corrections for Complete Models in 7- by 10-Foot Closed Rectangular Wind Tunnels. NACA ARR No. L5G31, 1945.

4. Thom, A.: Blockage Corrections in a Closed High-Speed Tunnel. R. & M. No. 2033, British A.R.C., 1943.

5. Toll, Thomas A., and Queijo, M. J.: Approximate Relations and Charts for Low-Speed Stability Derivatives of Swept Wings. NACA TN No. 1581, 1948.

6. Bates, William R.: Collection and Analysis of Wind-Tunnel Data on the Characteristics of Isolated Tail Surfaces with and without End Plates. NACA TN No. 1291, 1947.

7. Purser, Paul E., Spearman, M. Leroy, and Bates, William R.: Preliminary Investigation at Low Speed of Downwash Characteristics of Small-Scale Sweptback Wings. NACA TN No. 1378, 1947.

8. Schlichting, H.: Calculation of the Influence of a Body on the Position of the Aerodynamic Centre of Aircraft with Sweptback Wings. TN No. Aero 1879, British R.A.E., March 1947.

9. Shortal, Joseph A., and Maggin, Bernard: Effect of Sweepback and Aspect Ratio on Longitudinal Stability Characteristics of Wings at Low Speeds. NACA TN No. 1093, 1946.

10. Levacic, I.: Rolling Moment Due to Sideslip. Part II - The Effect of Sweepback and Plan Form. Rep. No. Aero 2092, British R.A.E., Nov. 1945

11. Munk, Max M.: The Aerodynamic Forces on Airship Hulls. NACA Rep. No. 184, 1924.

TABLE I

PHYSICAL CHARACTERISTICS OF THE MODELS

Center-of-gravity position, percent of M.A.C. 25

Horizontal tail:
- Area, sq ft 1.625
- Span, ft 2.85
- Aspect ratio 5
- Section . . . . . NACA 65-008

Vertical tail:
- Area, excluding dorsal, sq ft 1.600
- Aspect ratio 2.4
- Section . . . . . NACA 65-008

Wing:
- Section . . . . . NACA 65-110
- Incidence, deg 0

Λ (deg)	Area (sq ft)	Span (ft)	M.A.C. (ft)	Aspect ratio
-45	10.44	5.85	1.888	3.28
-30	9.60	7.17	1.460	5.36
-15	9.06	8.05	1.262	7.15
0_f	8.70	8.40	1.181	8.10
0_b	8.67	8.35	1.181	8.04
15	8.40	7.75	1.201	7.15
30	8.13	6.76	1.278	5.62
45	7.80	5.37	1.542	3.69

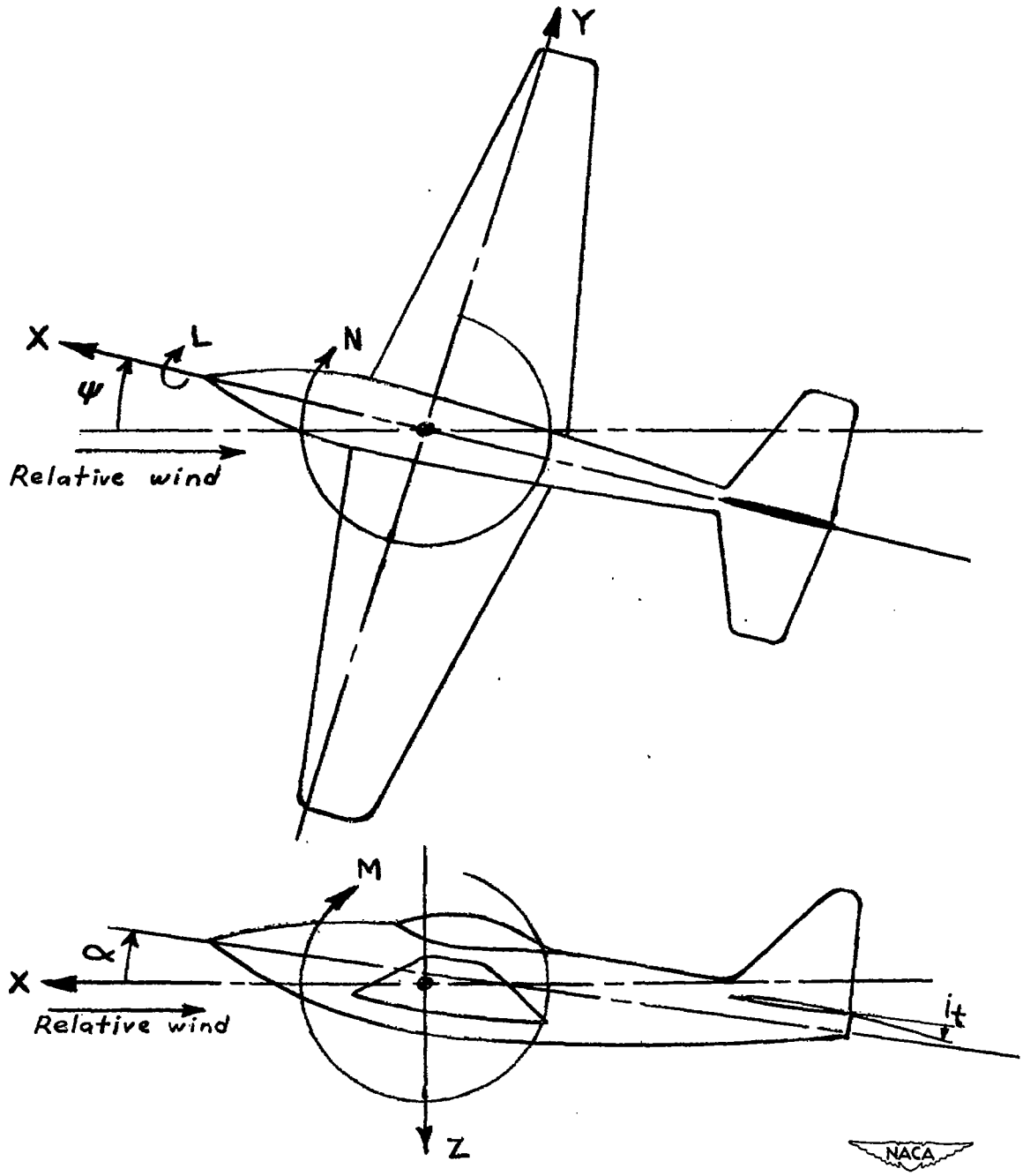

Figure 1.- System of stability axes showing positive values of forces, moments, and angles.

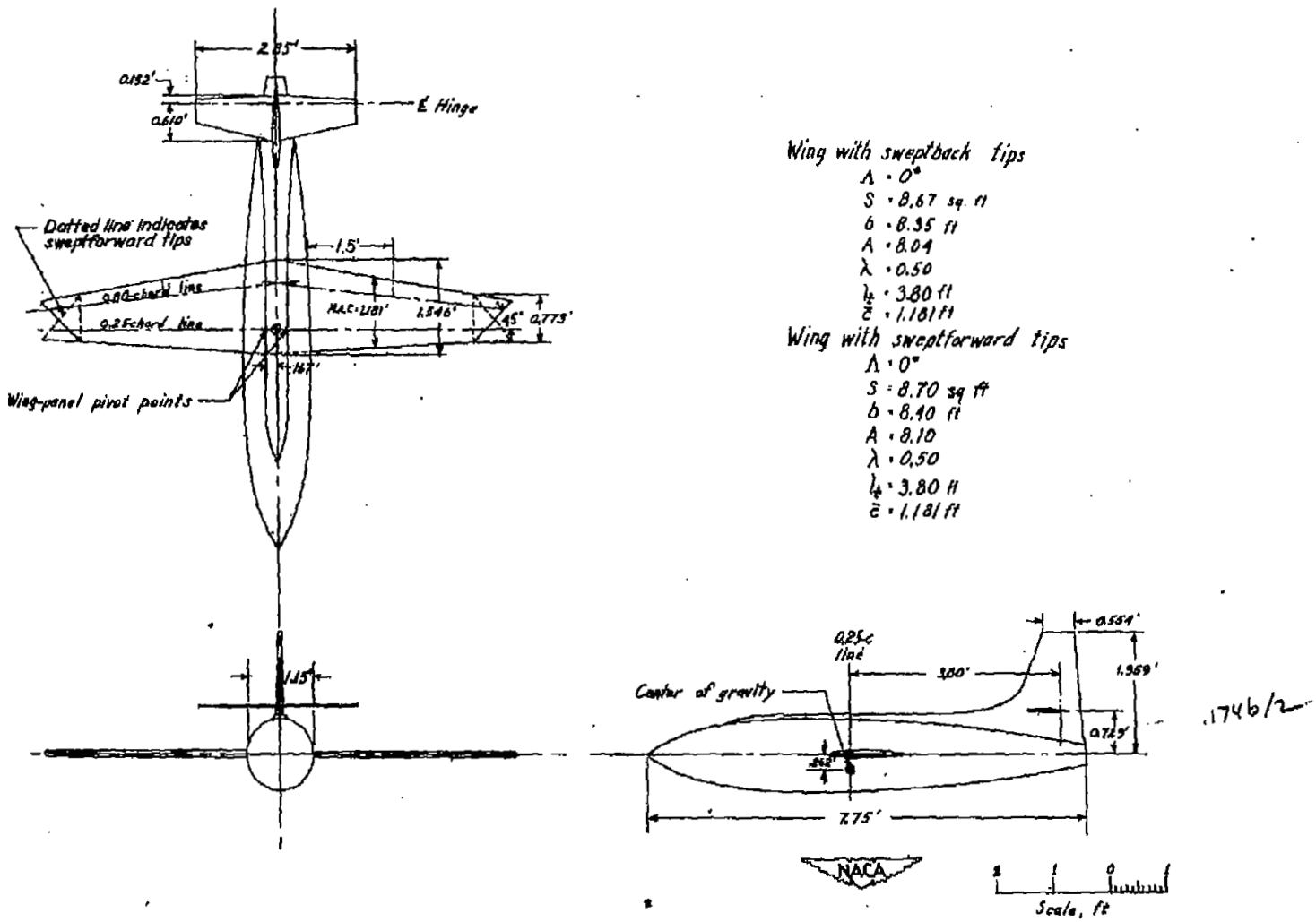

Figure 2.- Drawing of models with various swept-wing configurations.

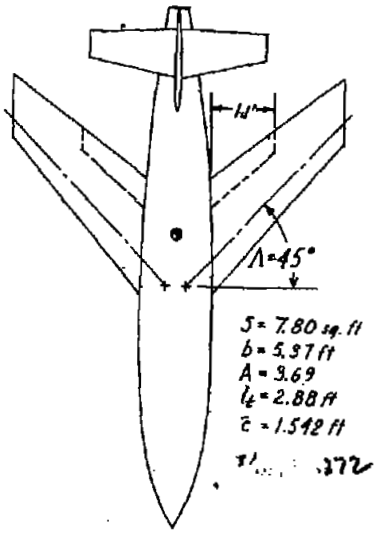
1.4'
Λ=45°
S = 7.80 sq. ft
b = 5.37 ft
A = 3.69
l_t = 2.88 ft
$\bar{c}$ = 1.542 ft
.272

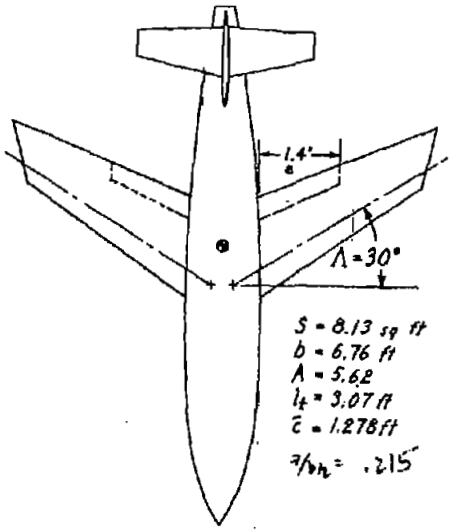
1.4'
Λ=30°
S = 8.13 sq ft
b = 6.76 ft
A = 5.62
l_t = 3.07 ft
$\bar{c}$ = 1.278 ft
.215

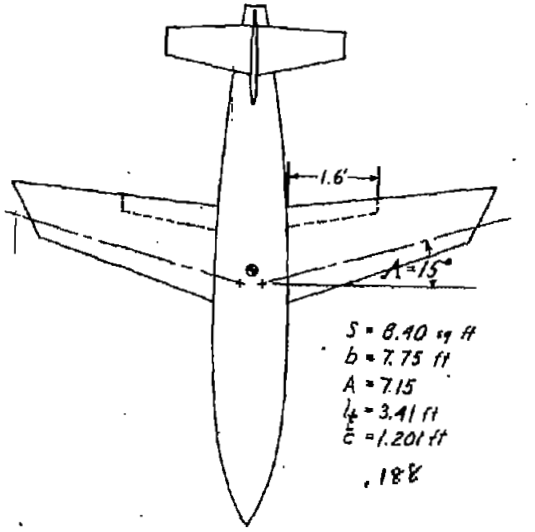
1.6'
Λ=15°
S = 8.40 sq ft
b = 7.75 ft
A = 7.15
l_t = 3.41 ft
$\bar{c}$ = 1.201 ft
.188

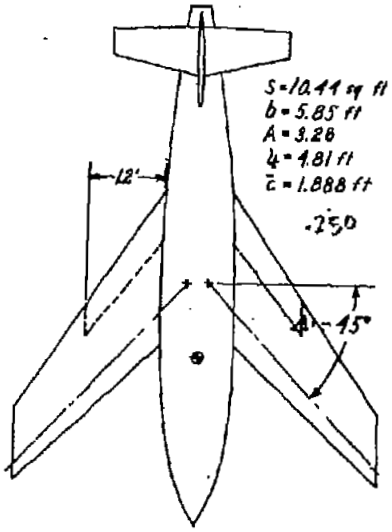
S = 10.44 sq ft
b = 5.85 ft
A = 3.28
l_t = 4.81 ft
$\bar{c}$ = 1.888 ft
.250
1.2'
Λ=45°

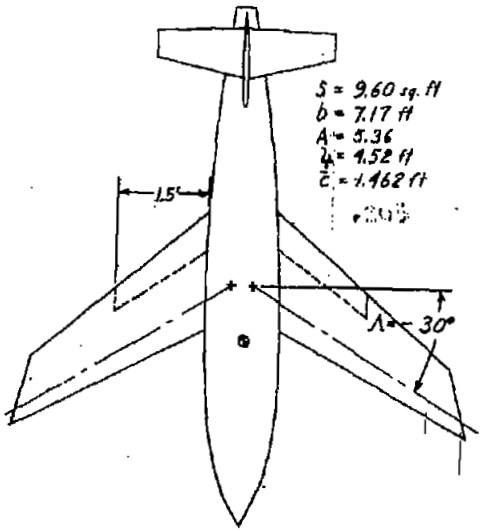
S = 9.60 sq. ft
b = 7.17 ft
A = 5.36
l_t = 4.52 ft
$\bar{c}$ = 1.462 ft
1.5'
Λ=30°

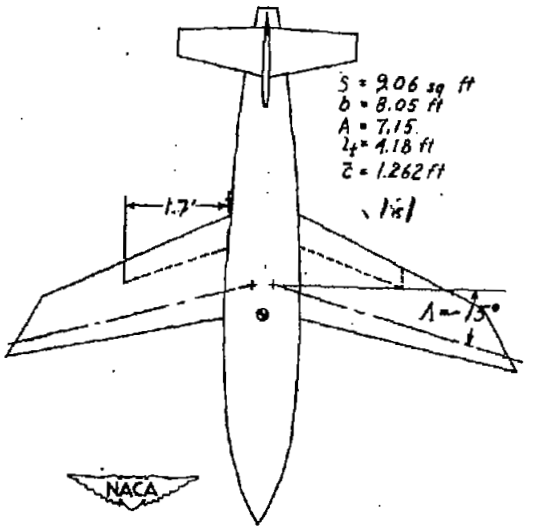
S = 9.06 sq ft
b = 8.05 ft
A = 7.15
l_t = 4.18 ft
$\bar{c}$ = 1.262 ft
.161
1.7'
Λ=15°
NACA

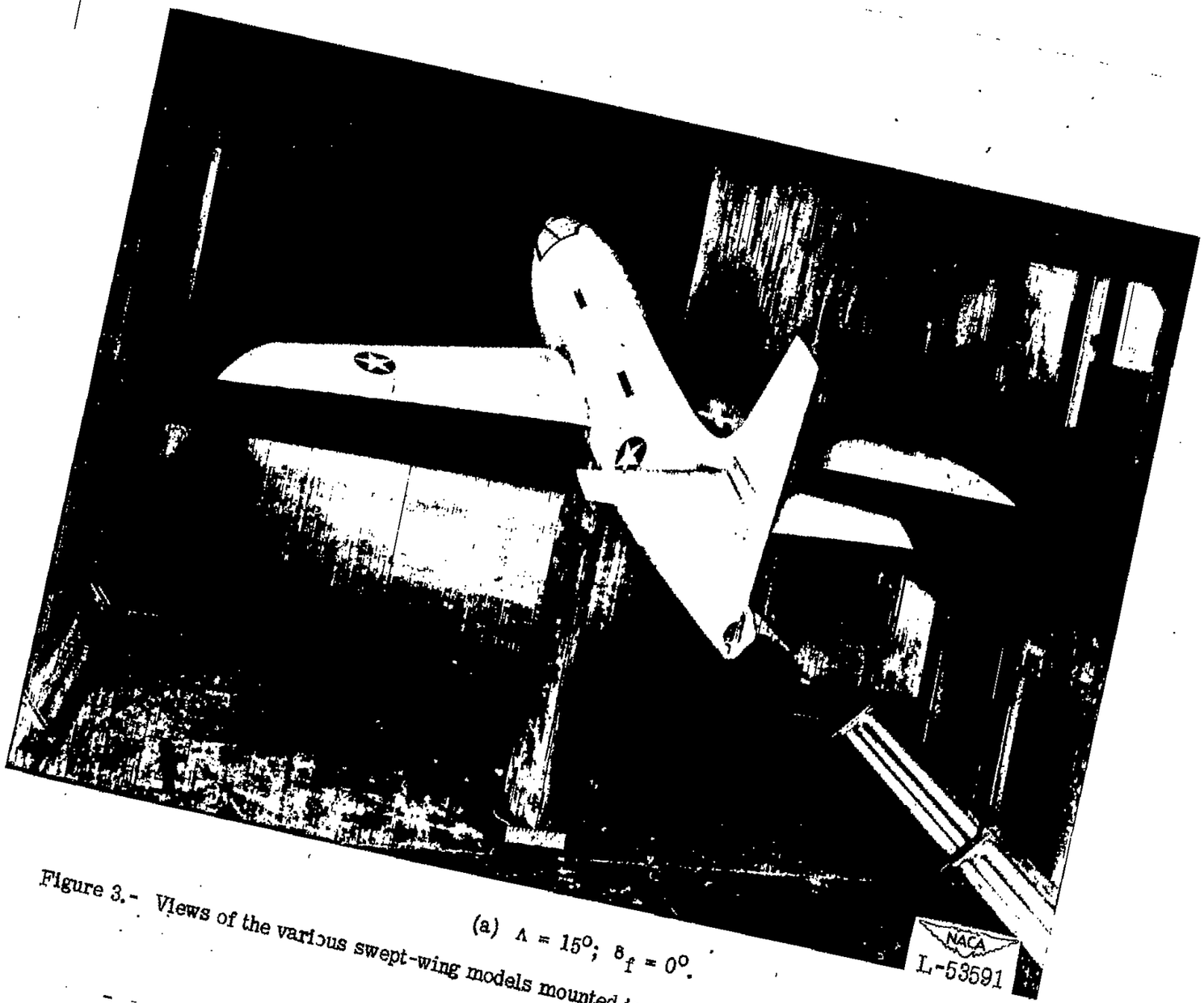

(a) $\Lambda = 15^{\circ}$; $\delta_f = 0^{\circ}$.

Figure 3.- Views of the various swept-wing models mounted in the Langley 300 MPH 7- by 10-foot tunnel.

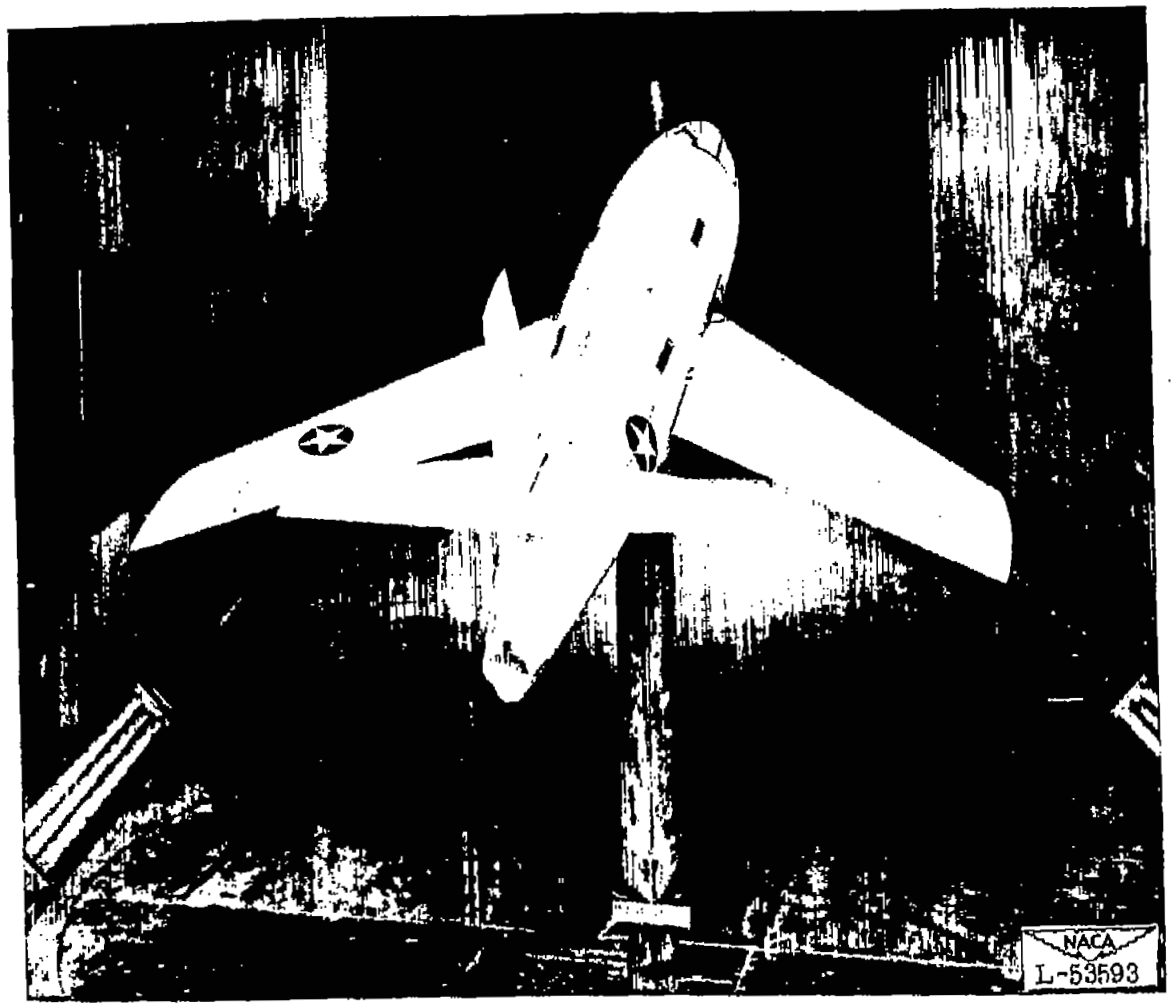

(b) $\Lambda = 45^{\circ}$; $\delta_f = 0^{\circ}$.

Figure 3.- Continued.

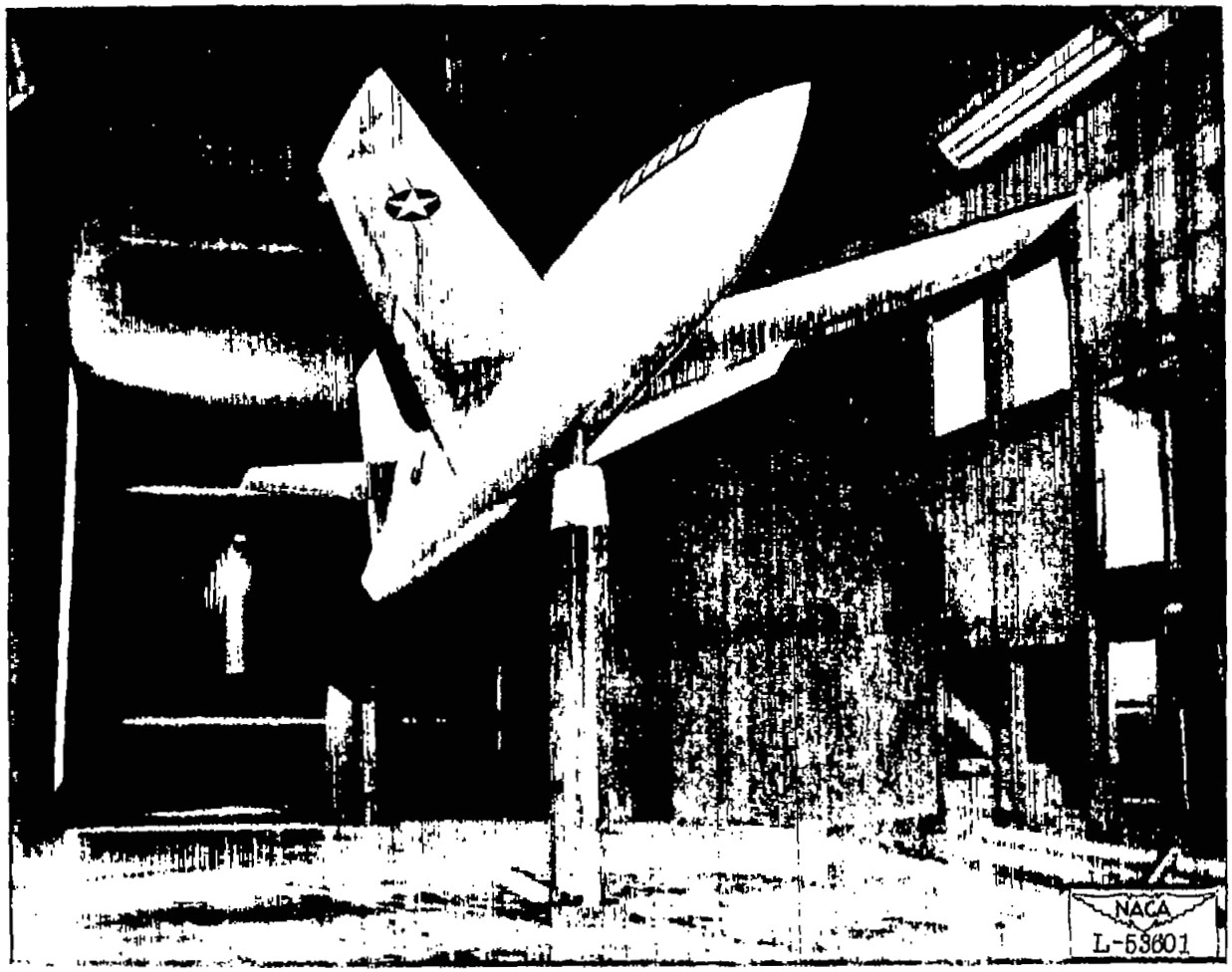

(c) $\Lambda = -45^{\circ}$; $\delta_f = 60^{\circ}$.

Figure 3.- Concluded.

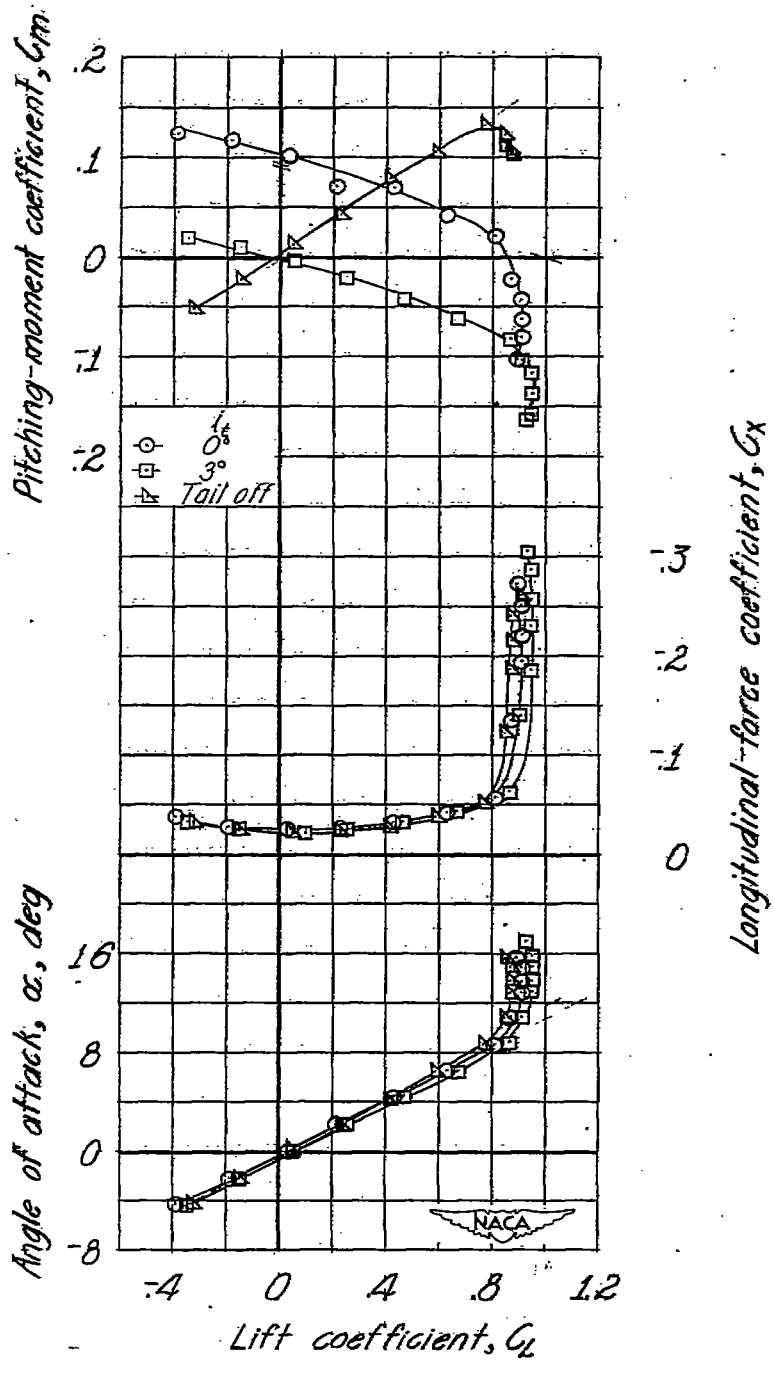

(a) $\Lambda = 0^\circ$.

Figure 4.- Aerodynamic characteristics for models with various swept wings, sweptback wing tips. $\delta_f = 0^\circ$.

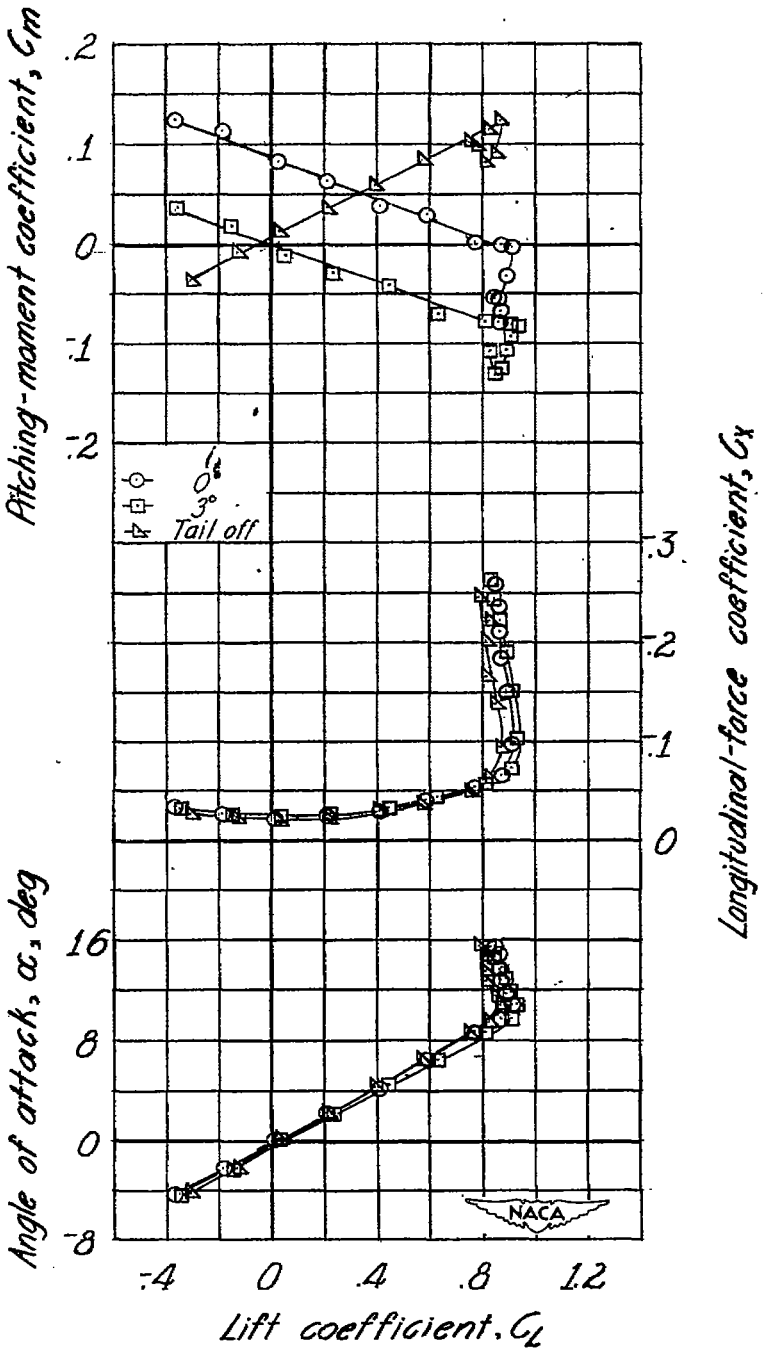

(b) $\Lambda = 15^{\circ}$.

Figure 4.- Continued.

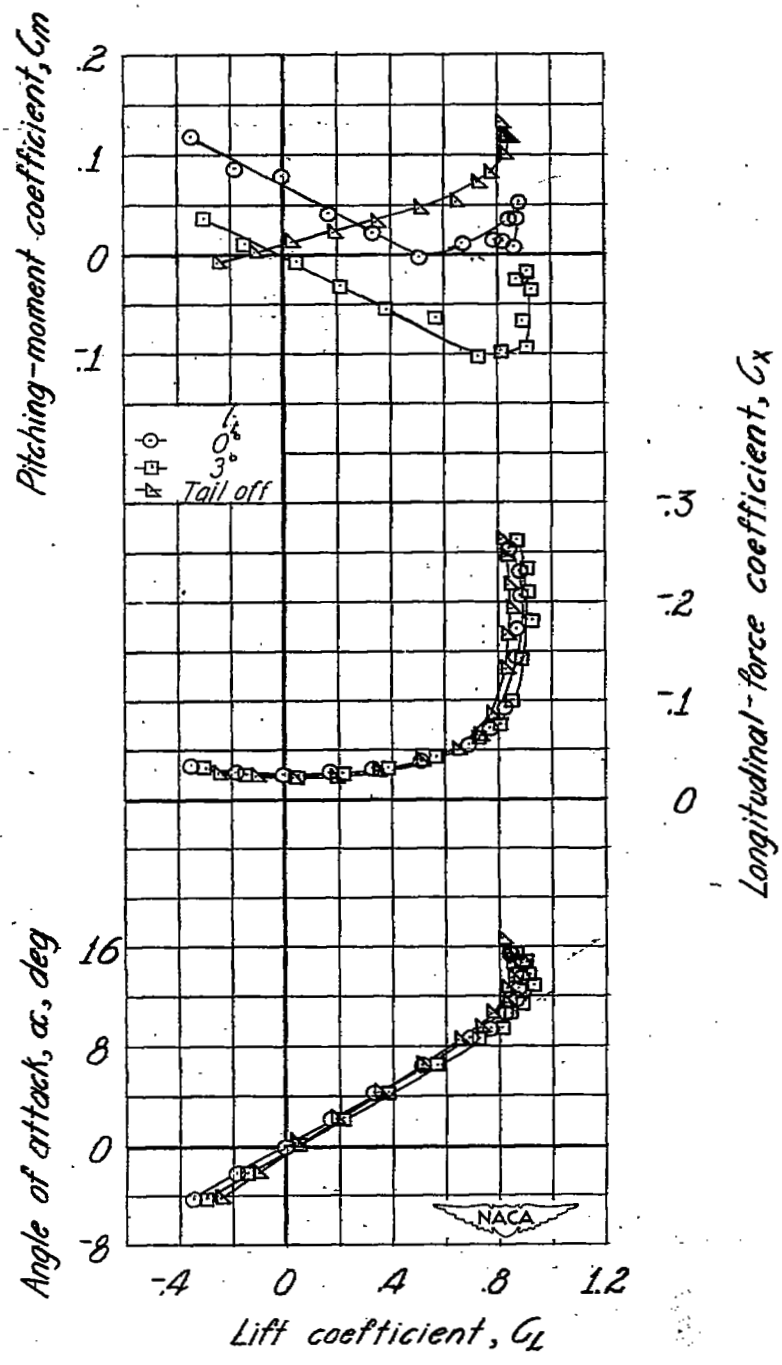

(c) $\Lambda = 30°$.

Figure 4.- Continued.

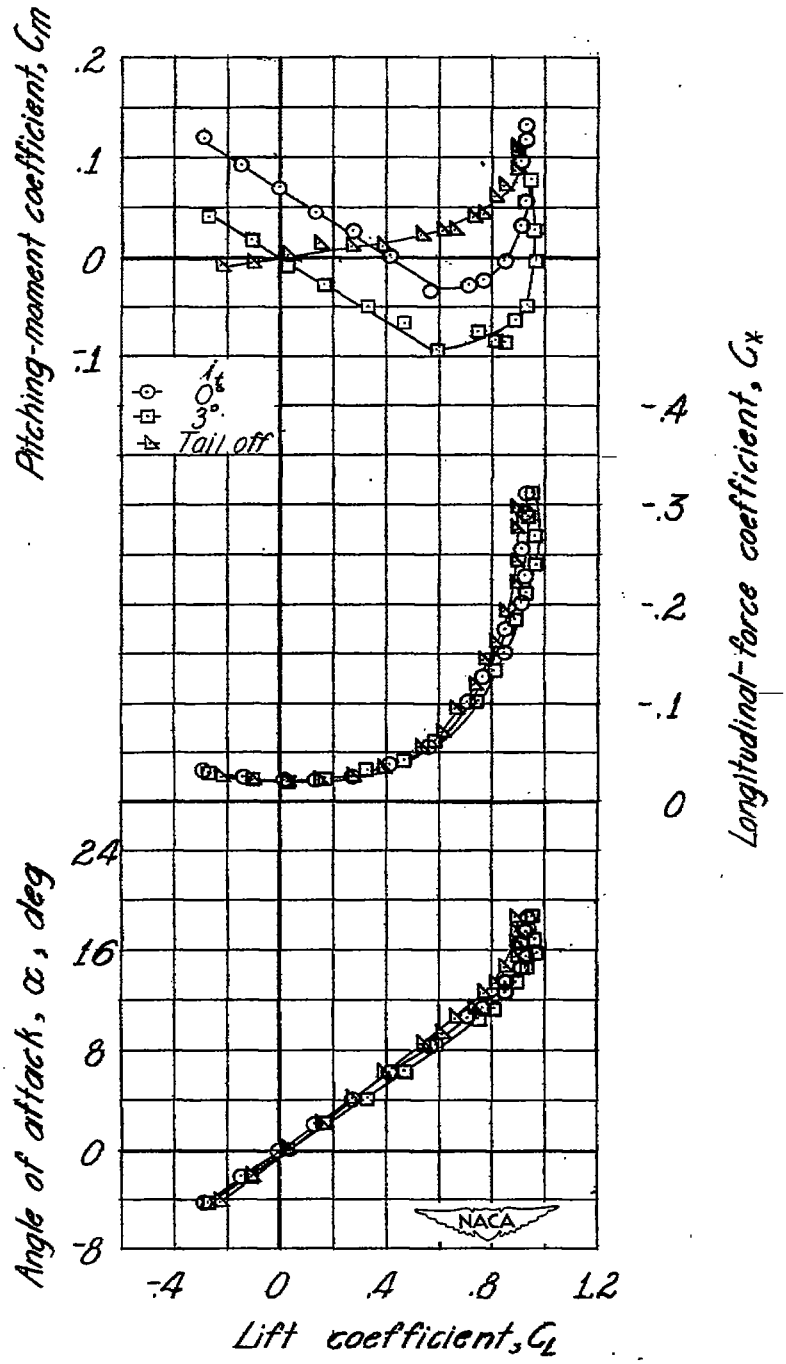

(d) $\Lambda = 45^\circ$.

Figure 4.- Concluded.

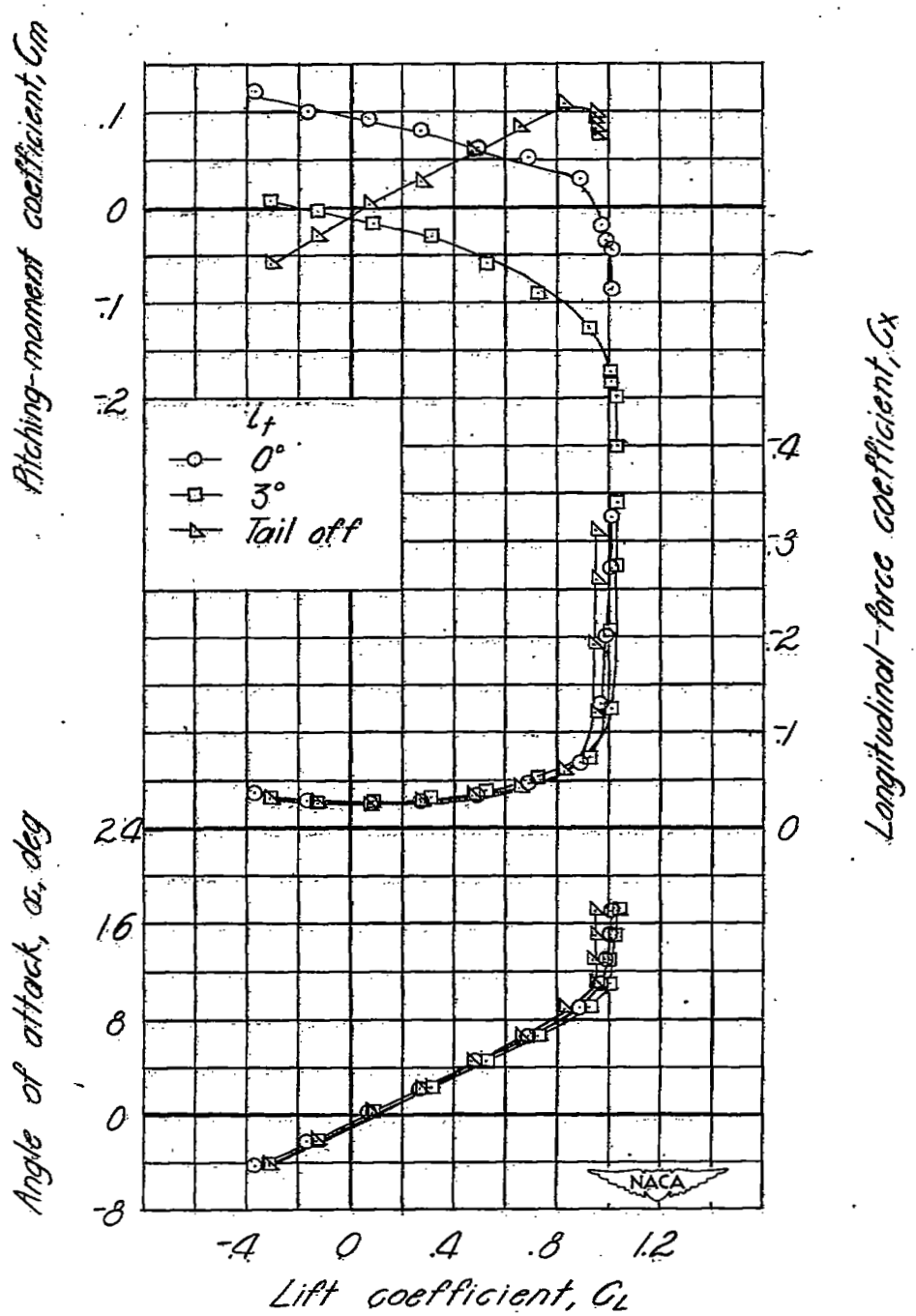

(a) $\Lambda = 0^\circ$.

Figure 5.- Aerodynamic characteristics for models with various swept wings, sweptforward wing tips. $\delta_f = 0^\circ$.

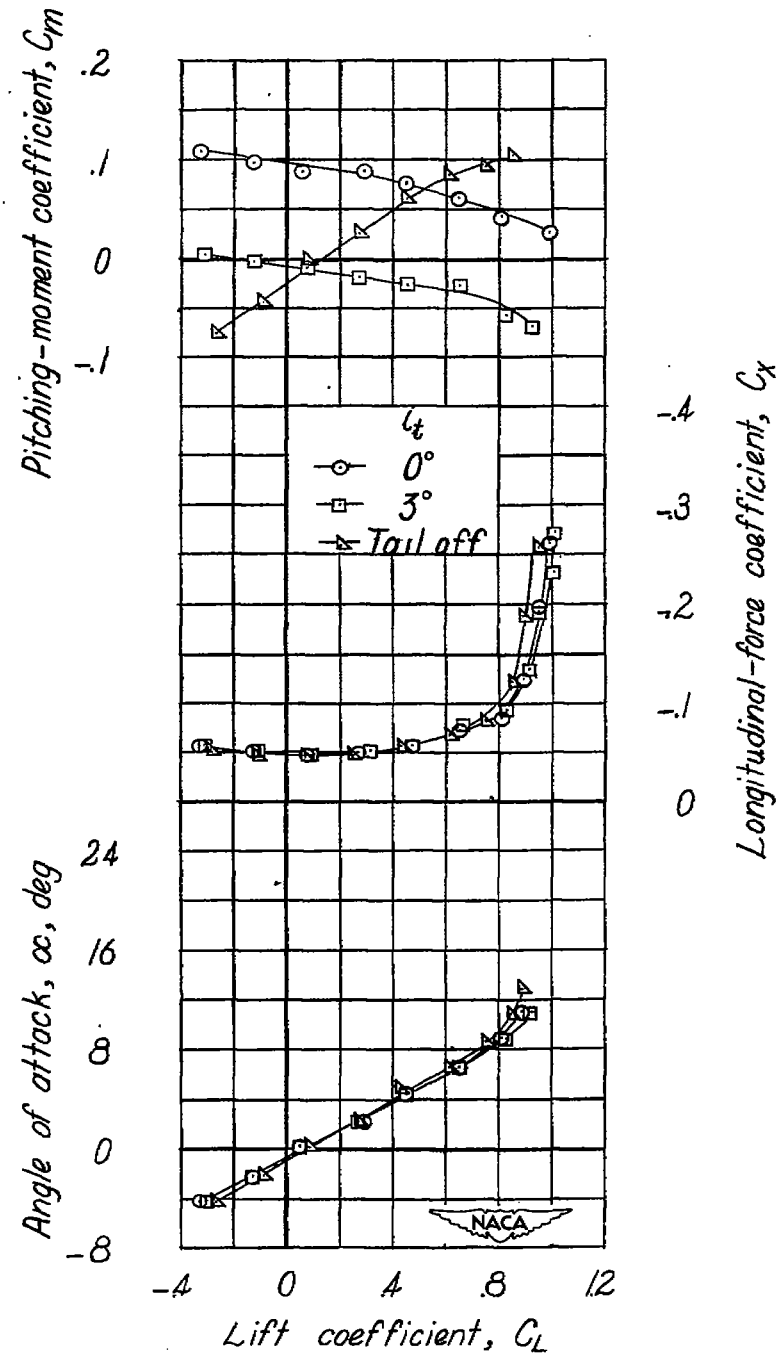

(b) $\Lambda = -15^\circ$.

Figure 5.- Continued.

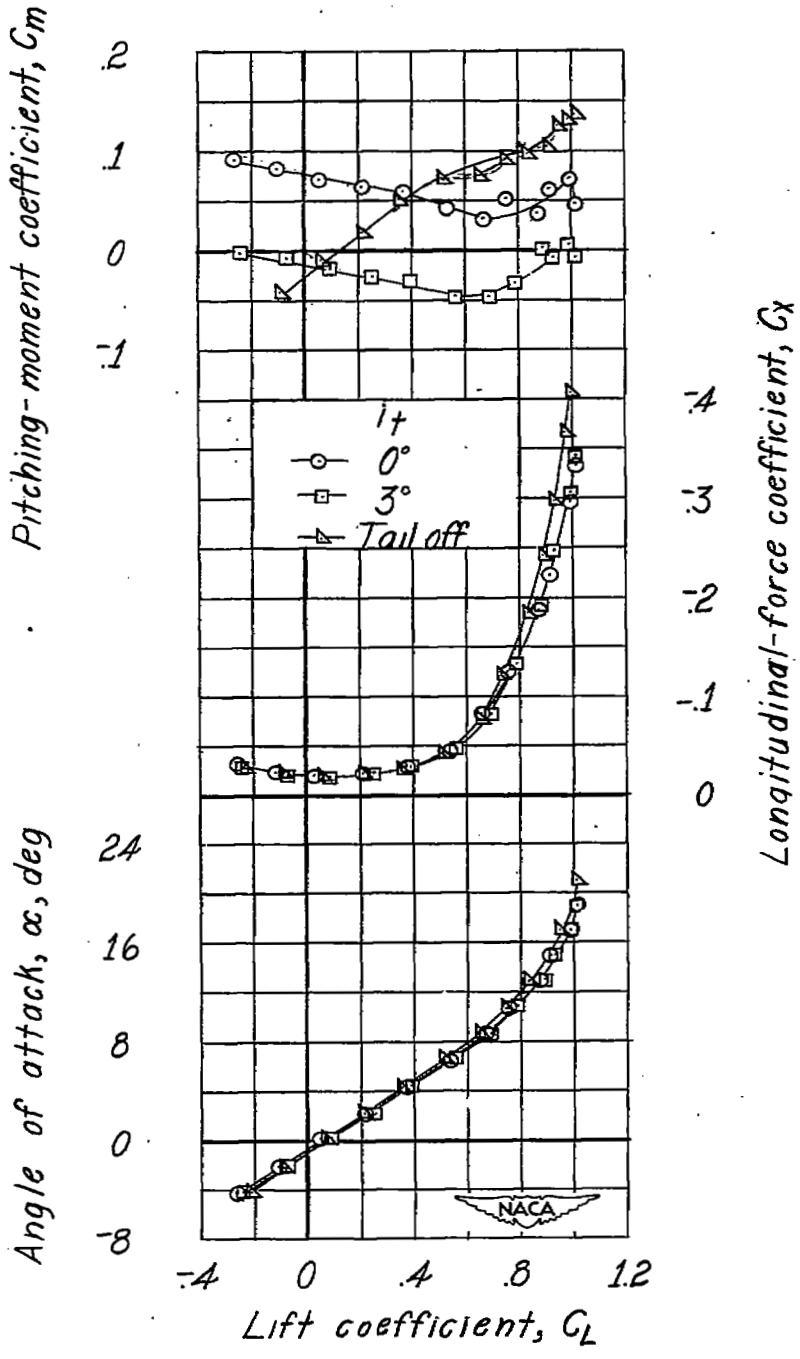

(c) $\Lambda = -30°$.

Figure 5.- Continued.

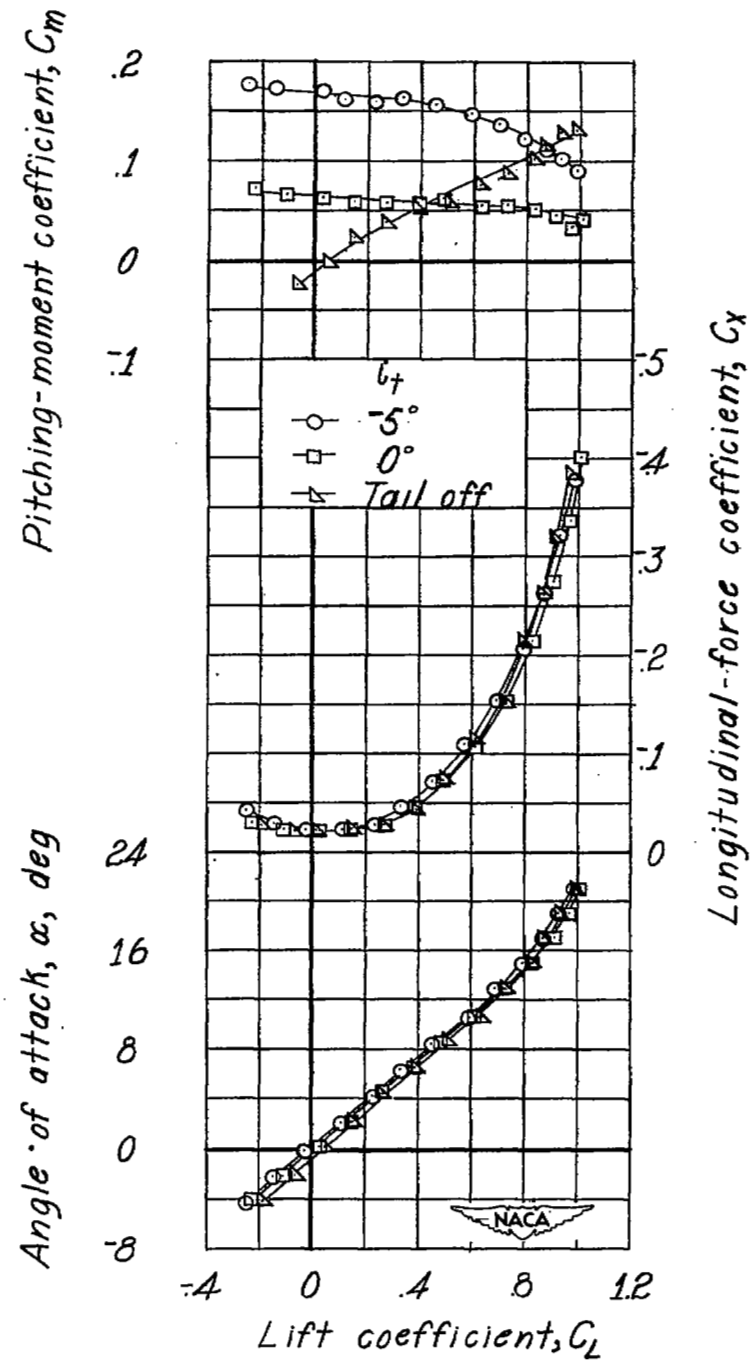

(d) $\Lambda = -45°$.

Figure 5.- Concluded.

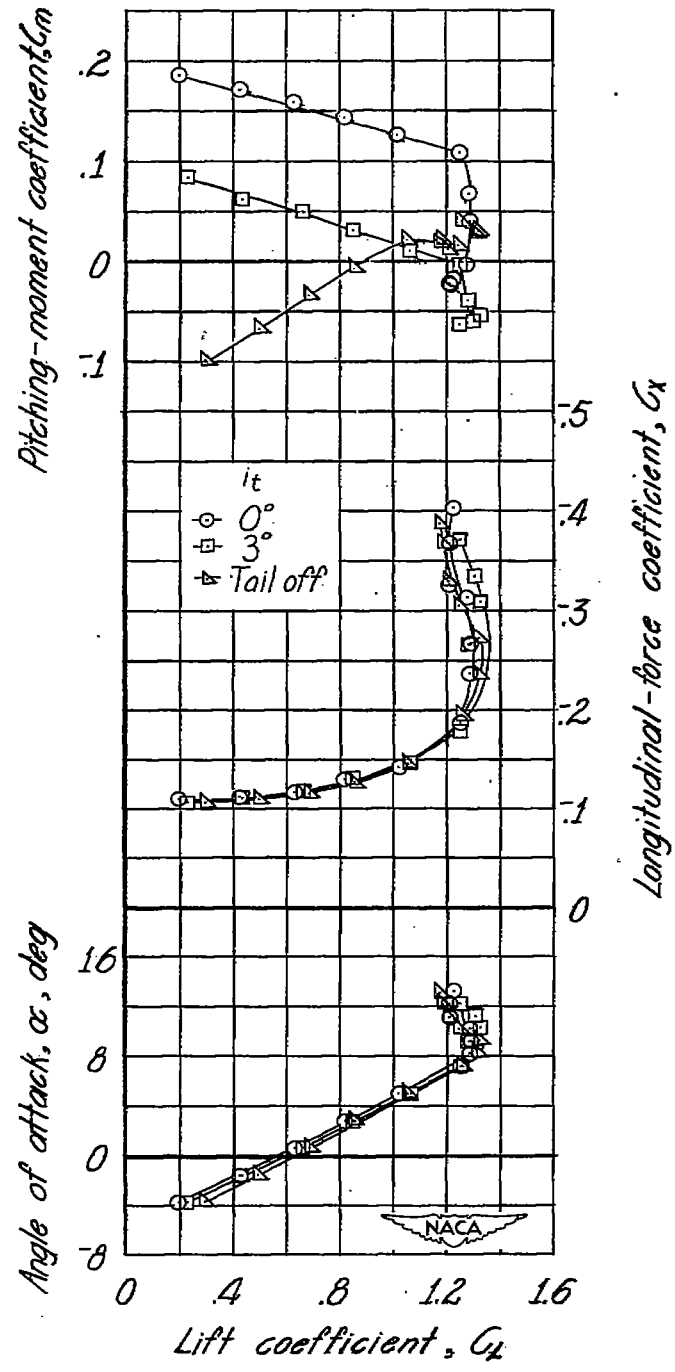

(a) $\Lambda = 0°$.

Figure 6.- Aerodynamic characteristics for models with various swept wings, swept-back tips. $\delta_f = 60°$.

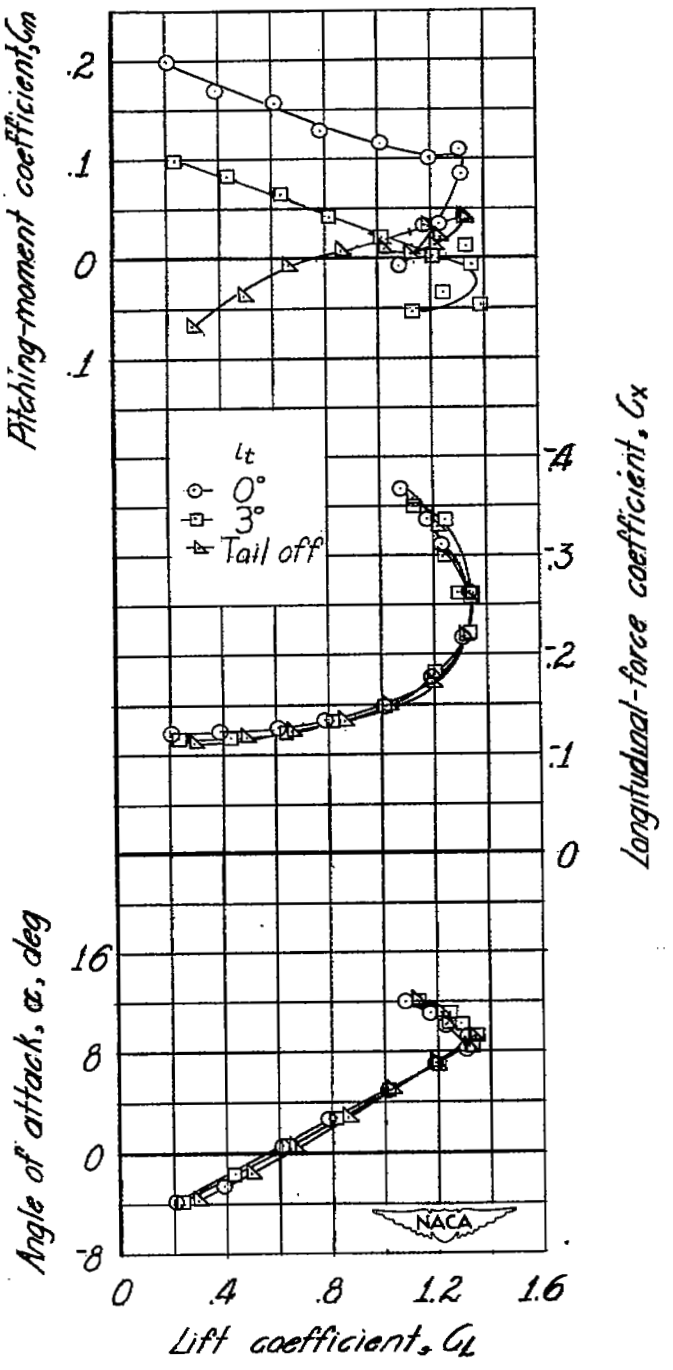

(b) $\Lambda = 15°$.

Figure 6.- Continued.

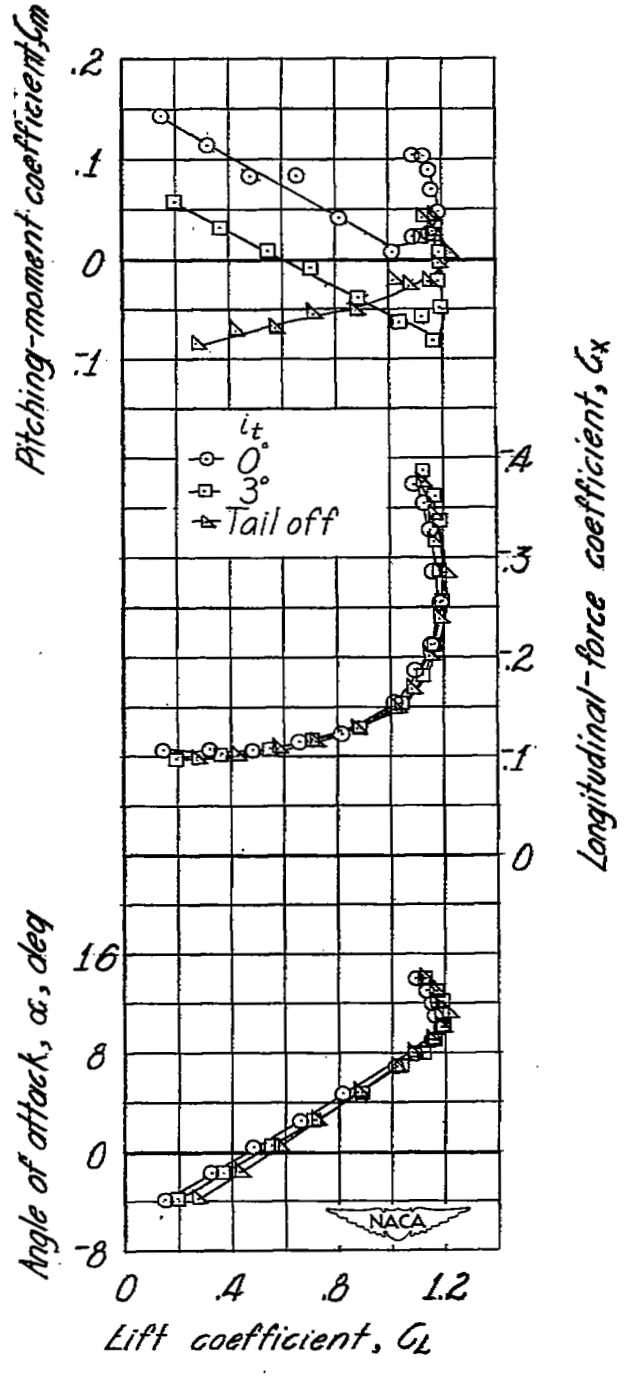

(c) $\Lambda = 30°$.

Figure 6.- Continued.

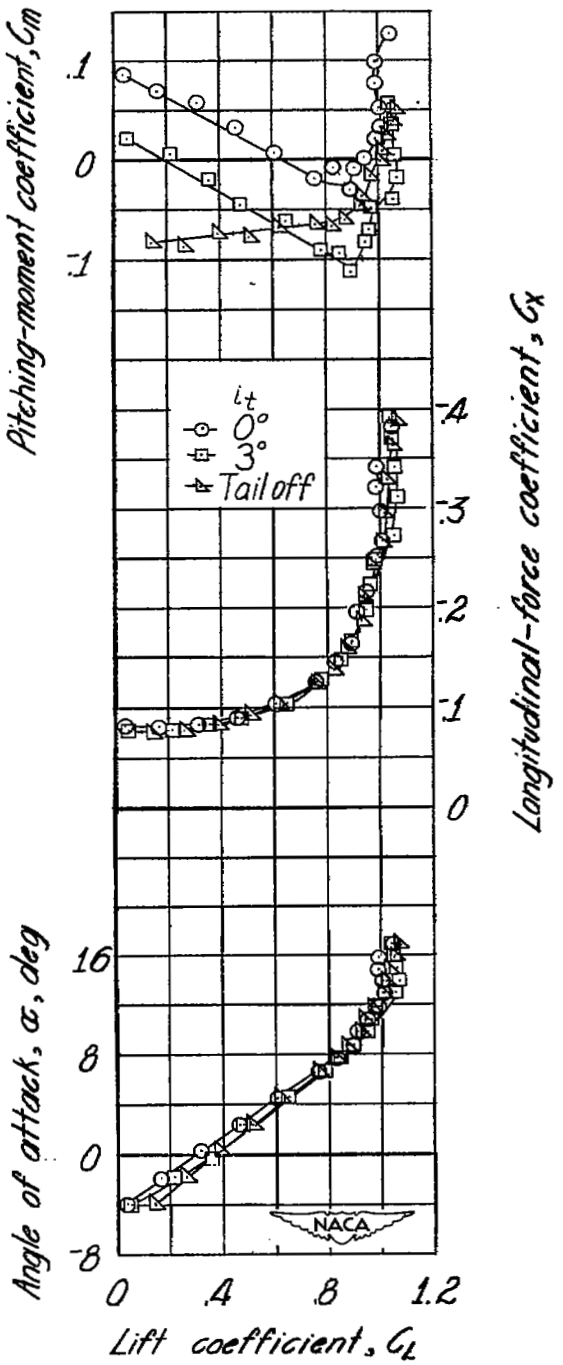

(d) $\Lambda = 45^{\circ}$.

Figure 6.- Concluded.

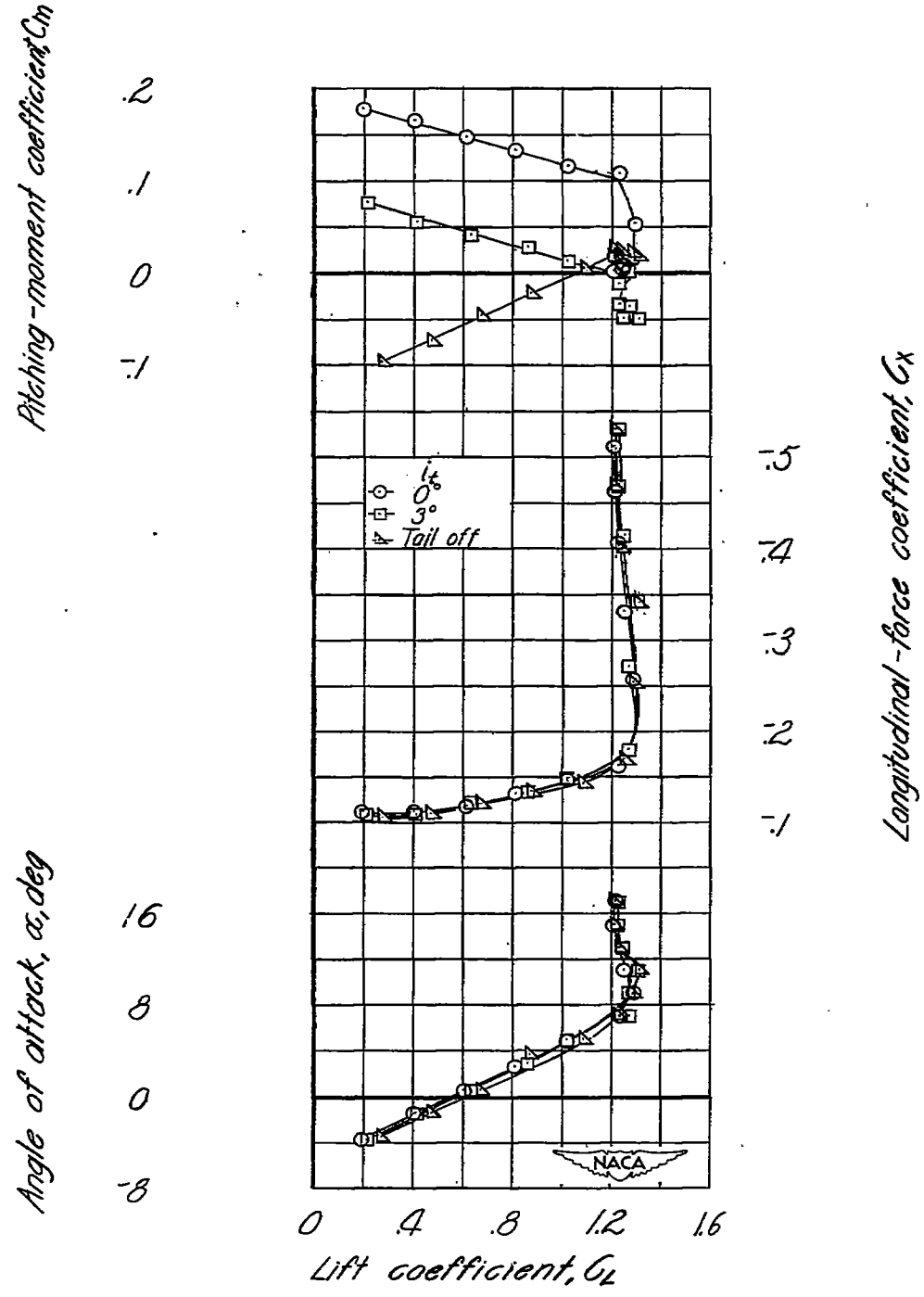

(a) $\Lambda = 0°$.

Figure 7.- Aerodynamic characteristics for models with various swept wings, sweptforward wing tips. $\delta_f = 60°$.

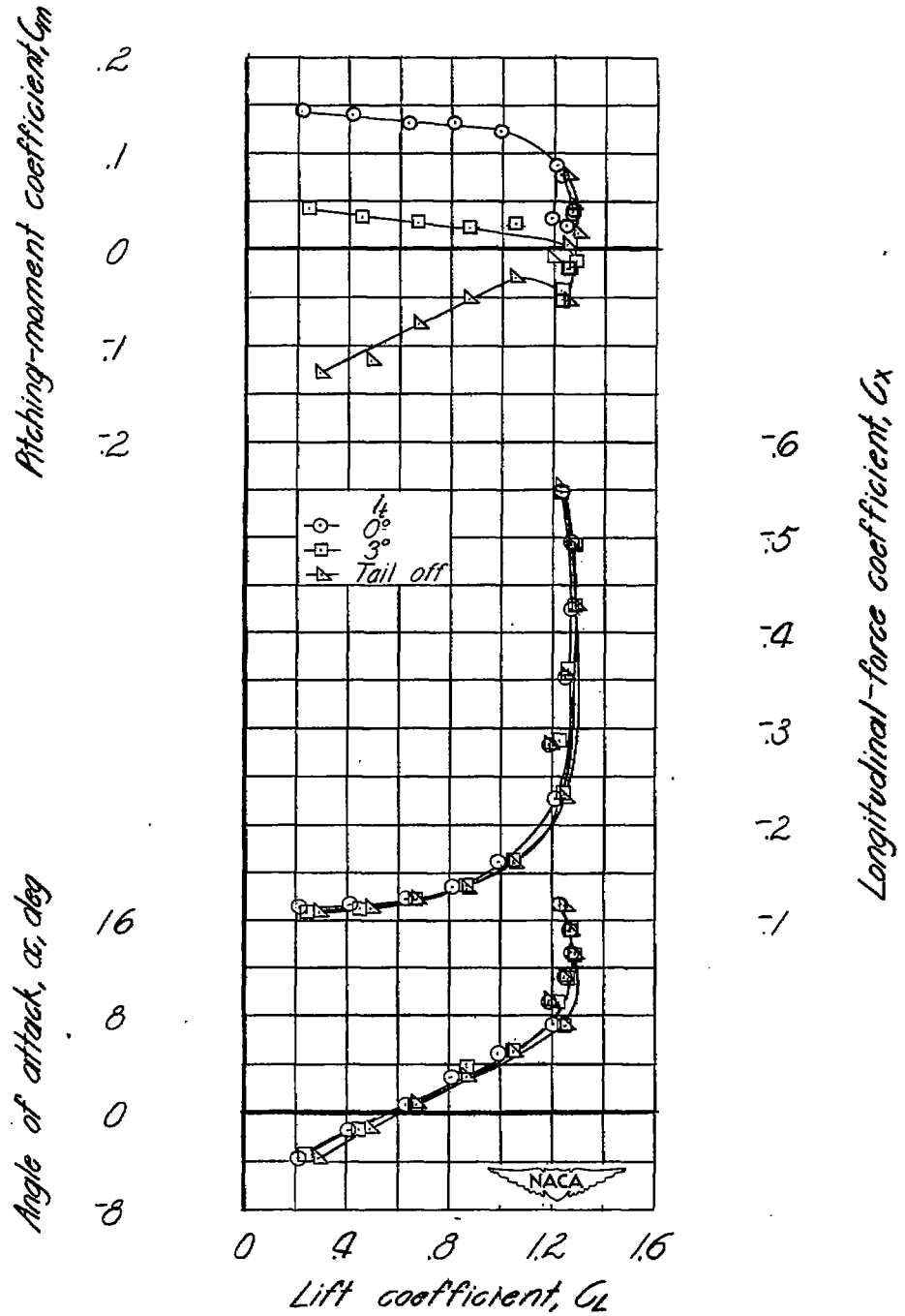

(b) $\Lambda = -15^{\circ}$.

Figure 7.- Continued.

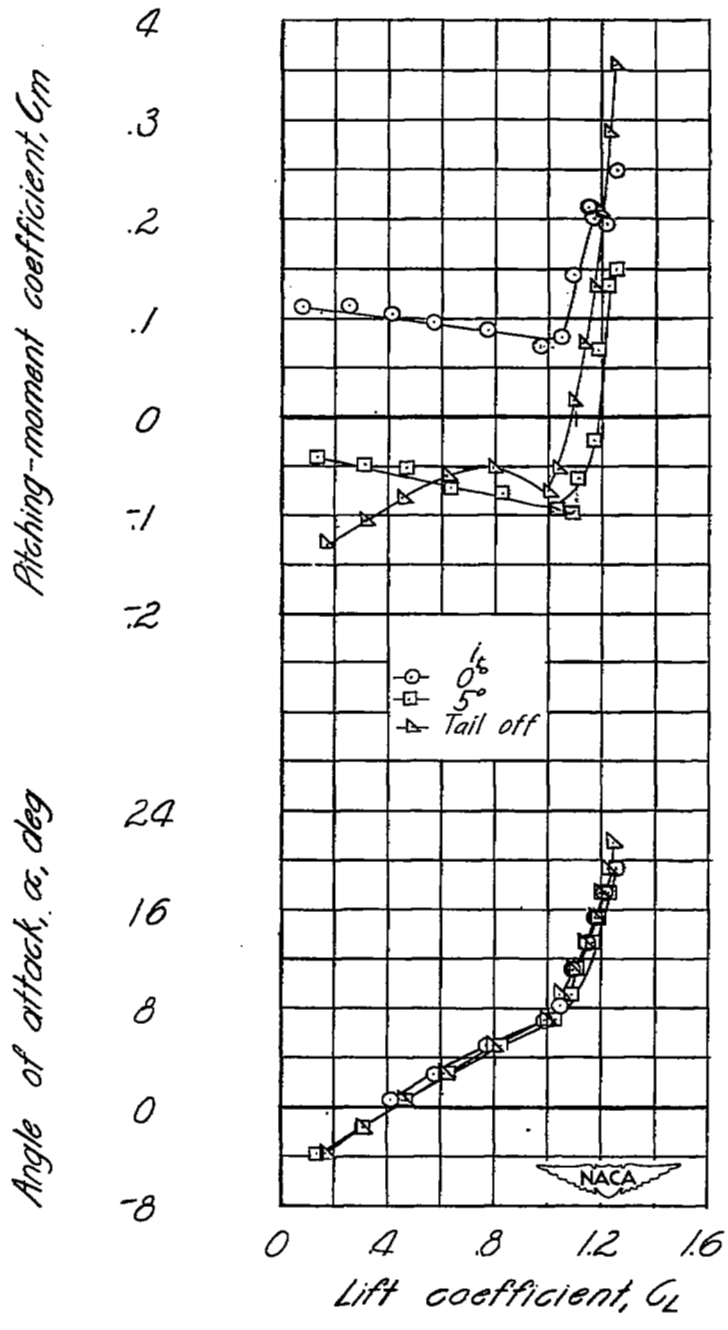

(c) $\Lambda = -30°$.

Figure 7.- Continued.

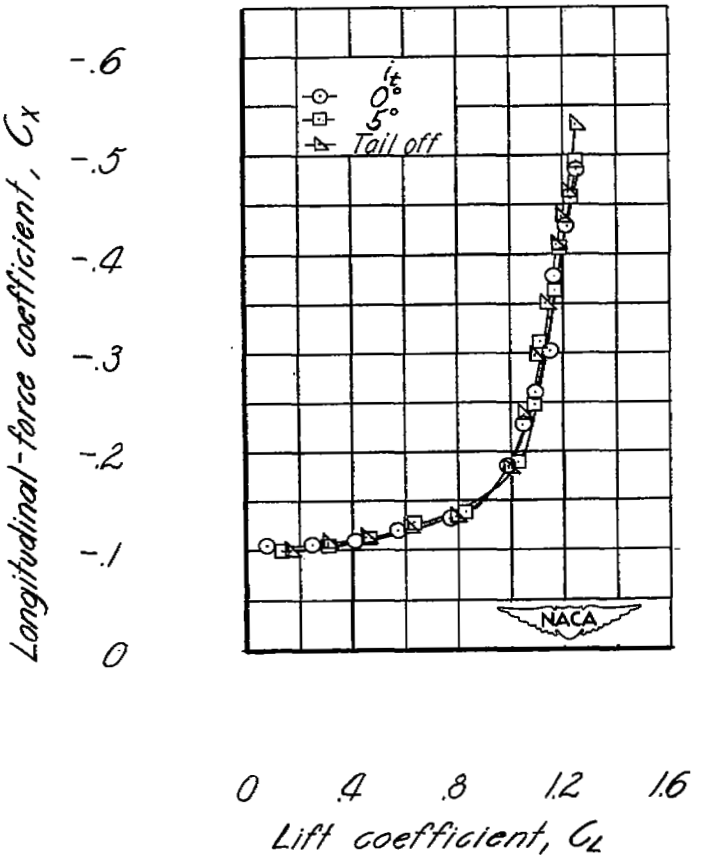

(c) Concluded.

Figure 7.- Continued.

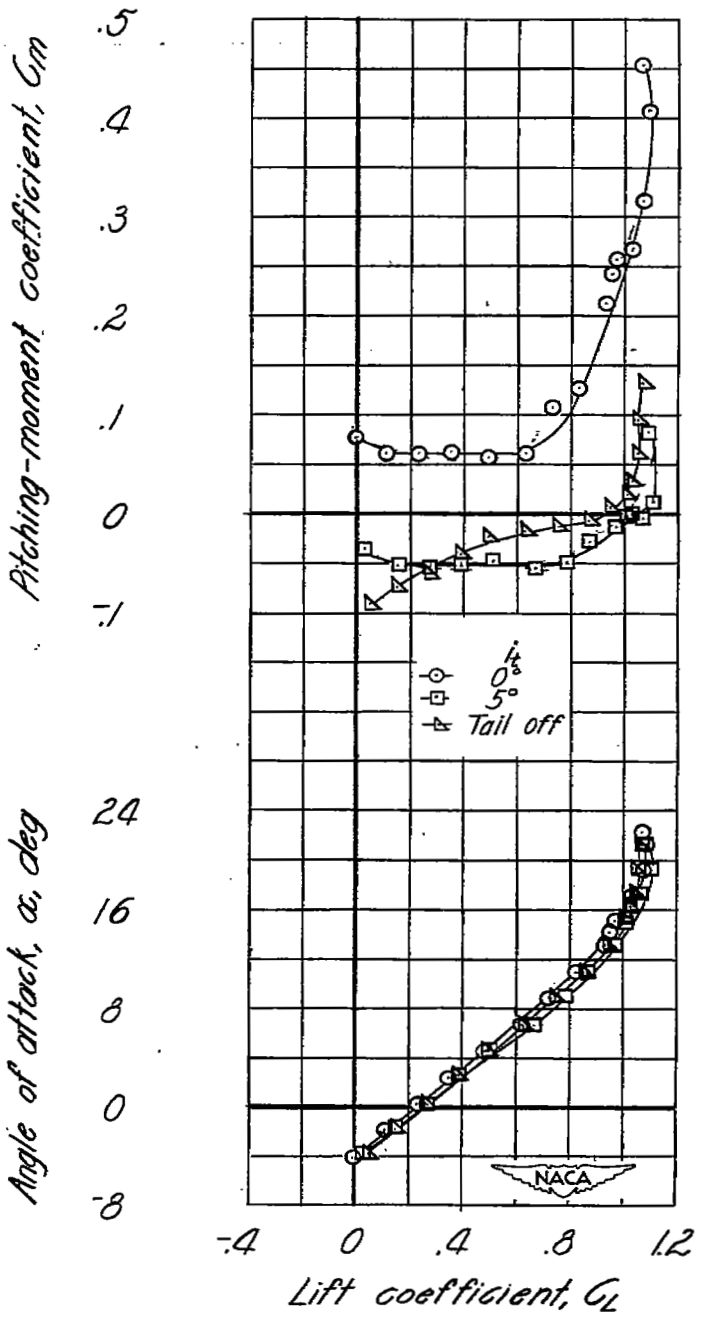

(d) $\Lambda = -45^\circ$.

Figure 7.- Continued.

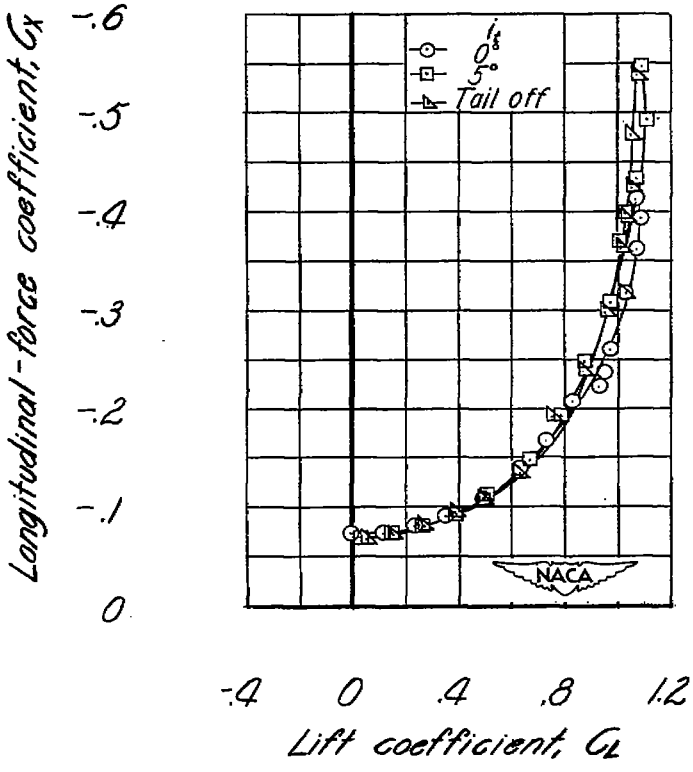

(d) Concluded.

Figure 7.- Concluded.

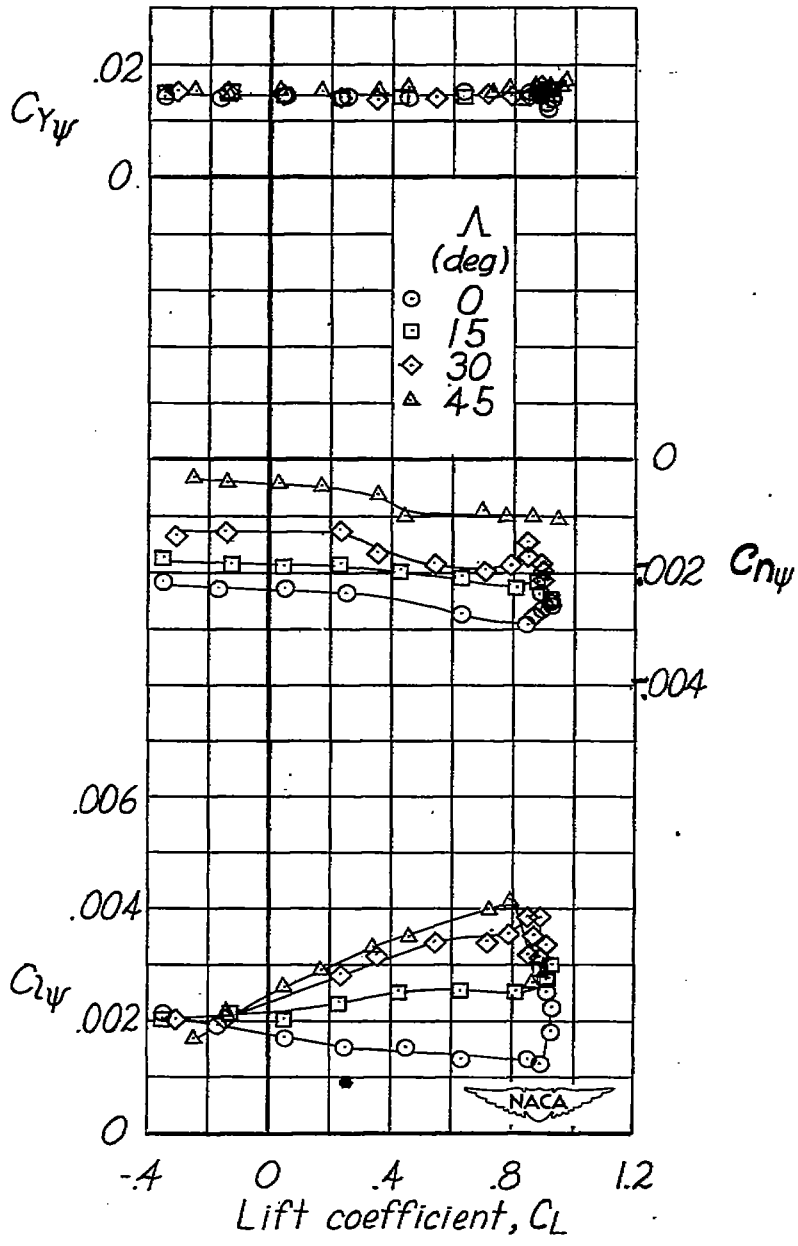

(a) Sweptback wings.

Figure 8.- Lateral-stability parameters for models with various swept wings. $\delta_f = 0°$.

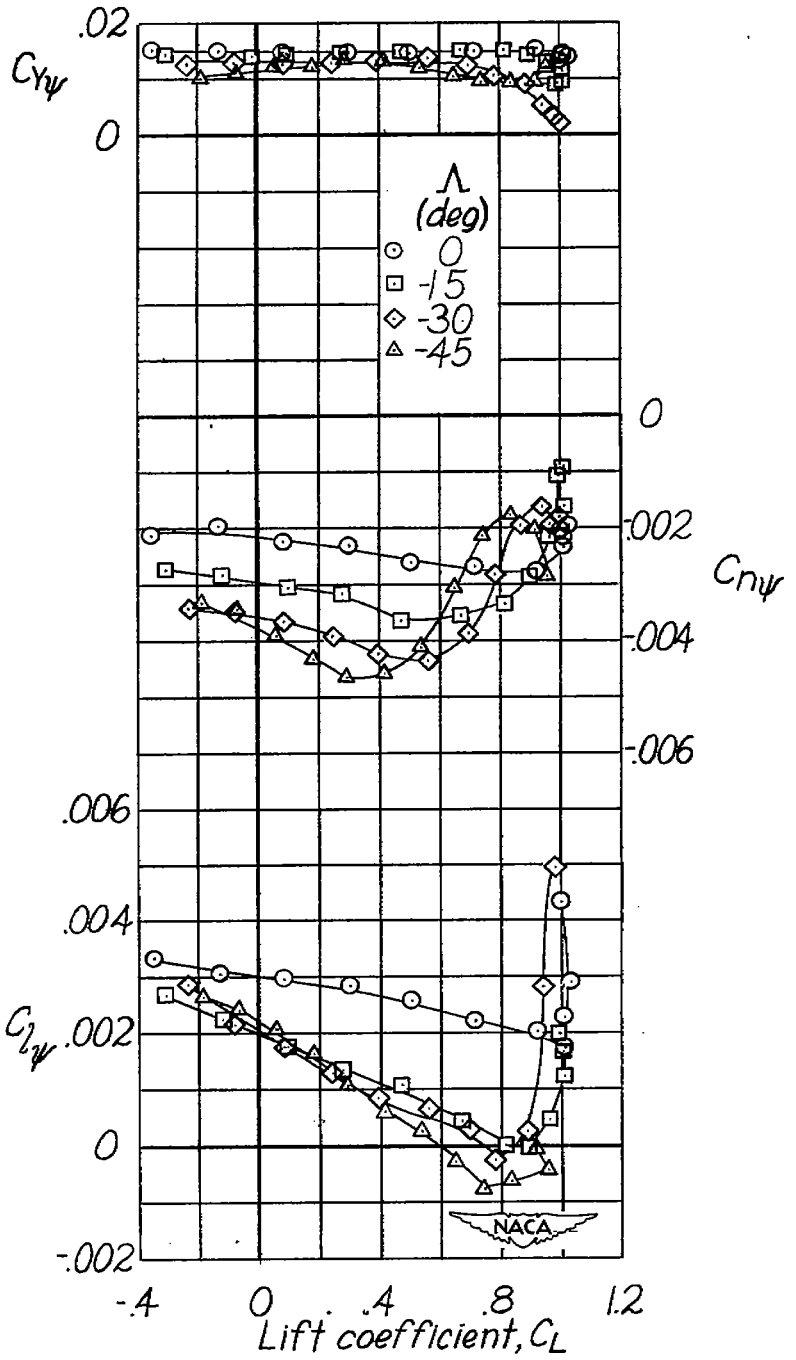

(b) Sweptforward wings.

Figure 8.- Concluded.

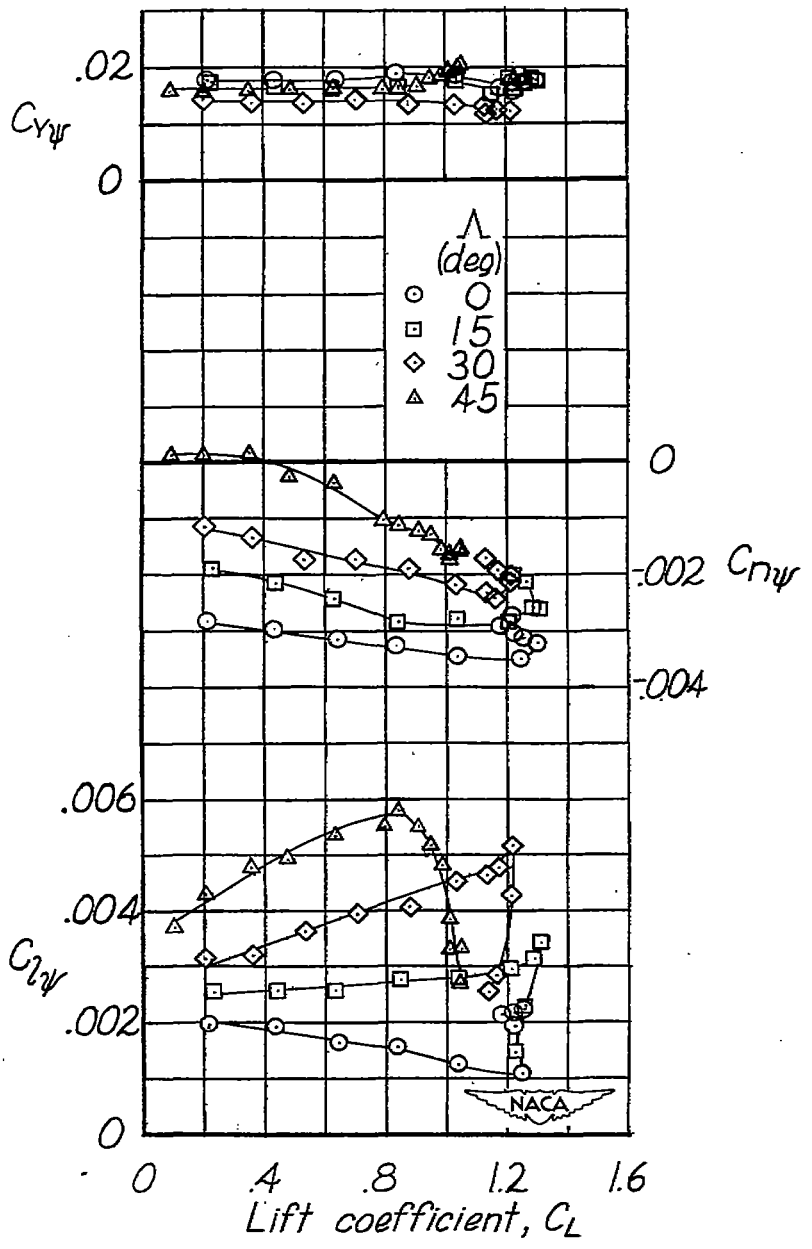

(a) Sweptback wings.

Figure 9.- Lateral-stability parameters for models with various swept wings. $\delta_f = 60°$.

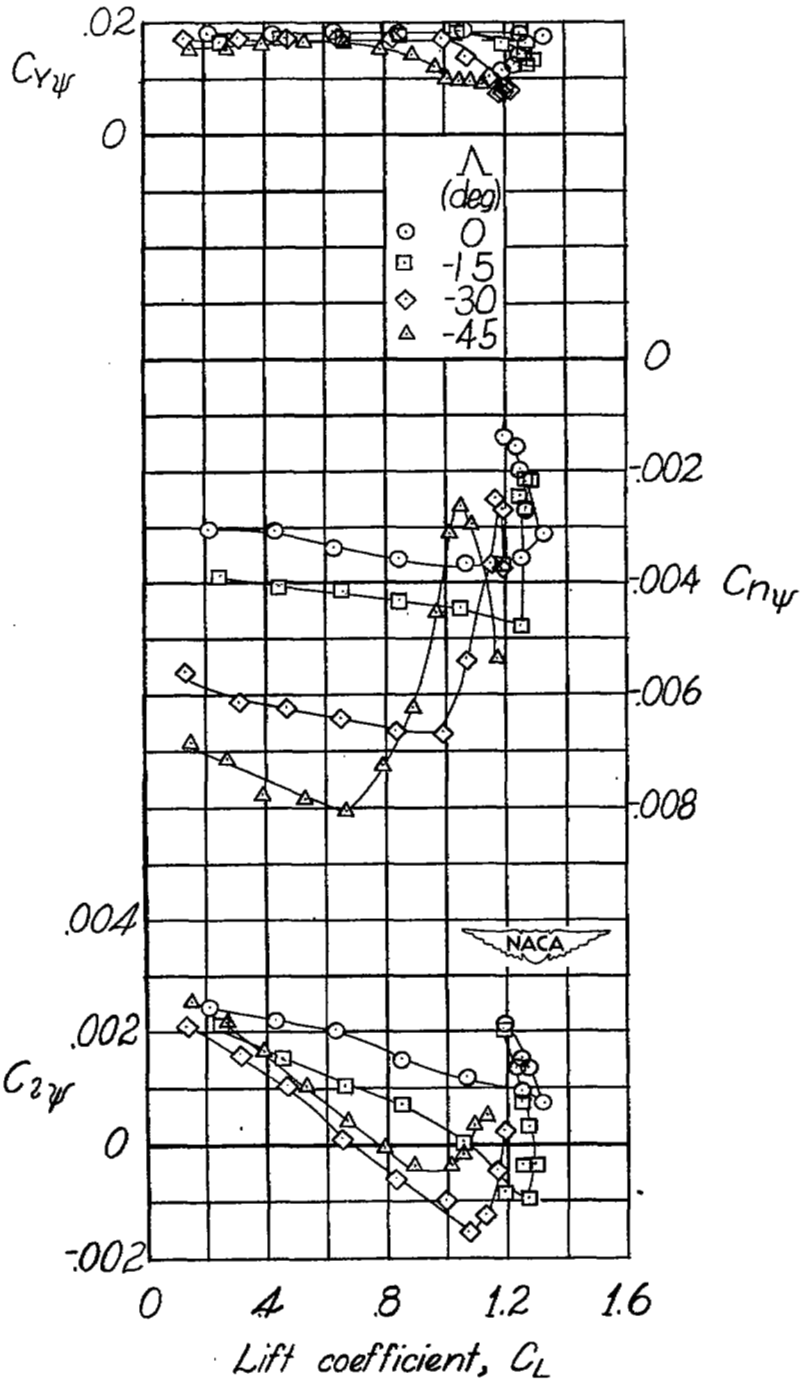

(b) Sweptforward wings.

Figure 9.- Concluded.

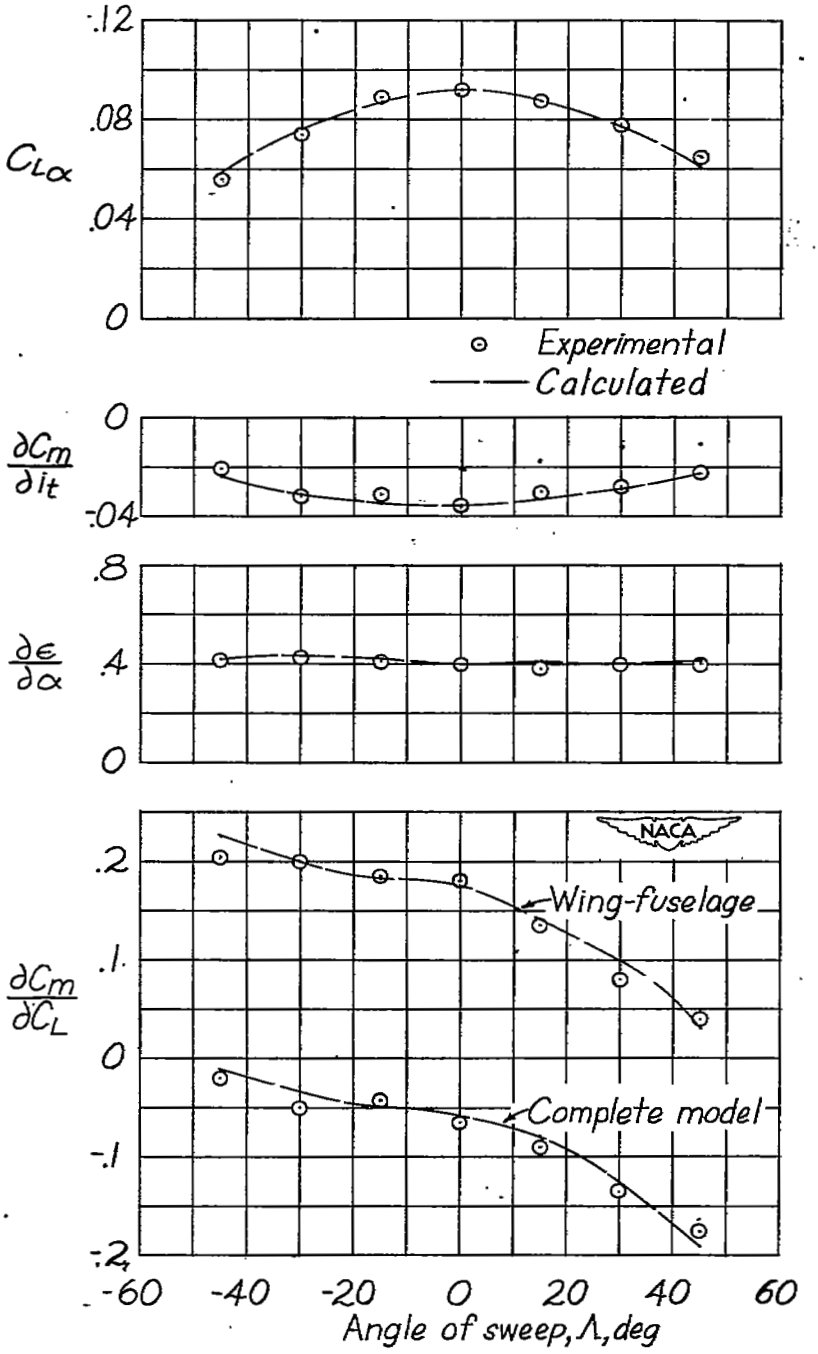

Figure 10.- Comparison of experimental and calculated values of static-longitudinal-stability determinants for models with various swept wings. $\delta_f = 0°$.

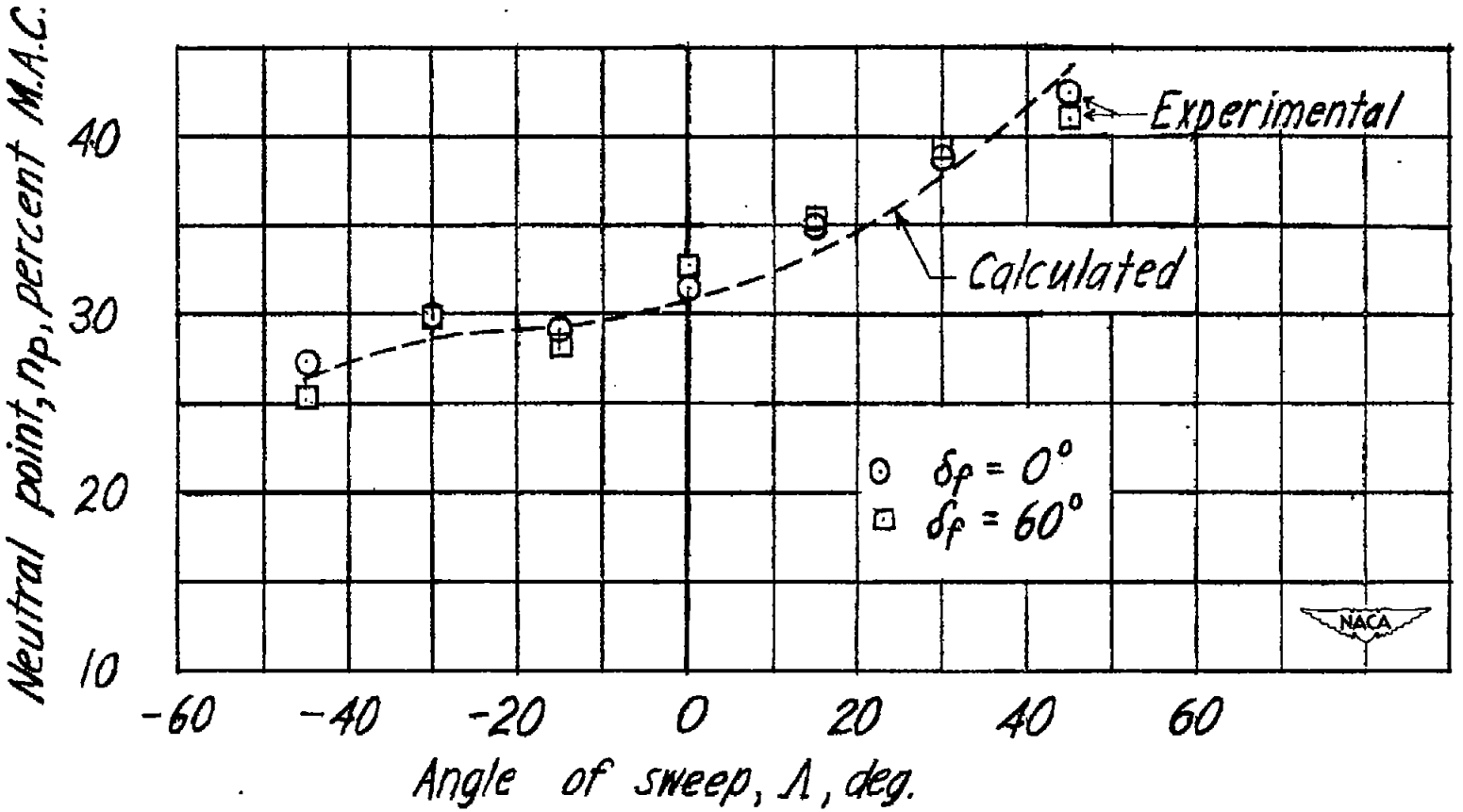

Figure 11.- Effect of sweep on the neutral-point location for models with various swept wings.

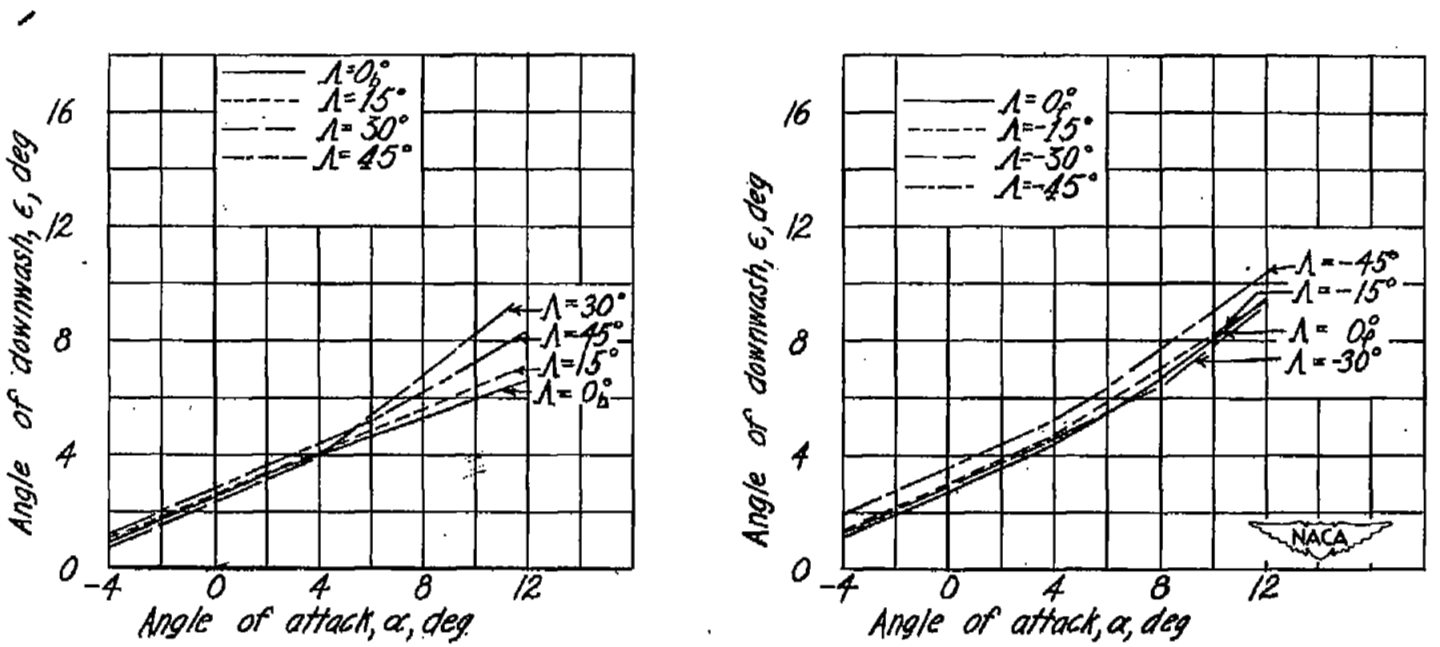

(a) Sweptback wings.

(b) Sweptforward wings.

Figure 12.- Variation of downwash angle with angle of attack for models with various swept wings. $\delta_f = 0°$.

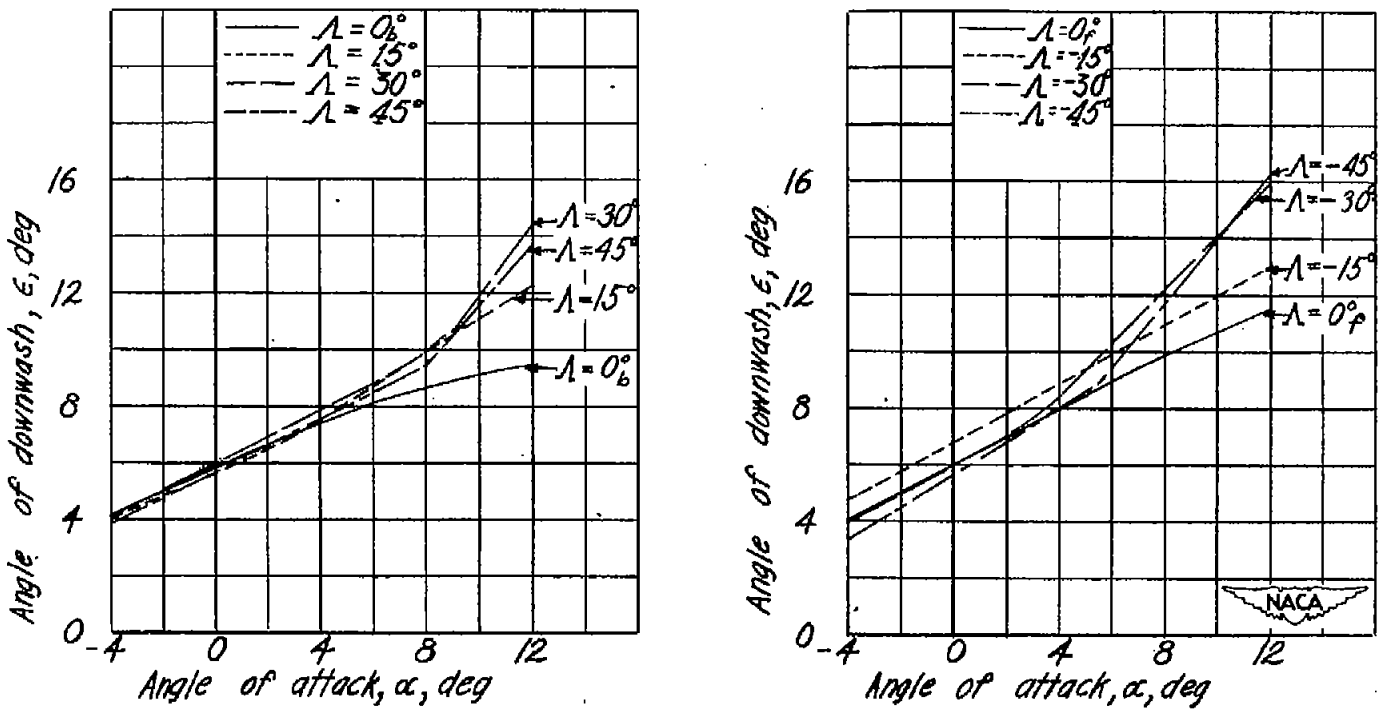

(a) Sweptback wings.

(b) Sweptforward wings.

Figure 13.- Variation of downwash angle with angle of attack for models with various swept wings. $\delta_f = 60°$.

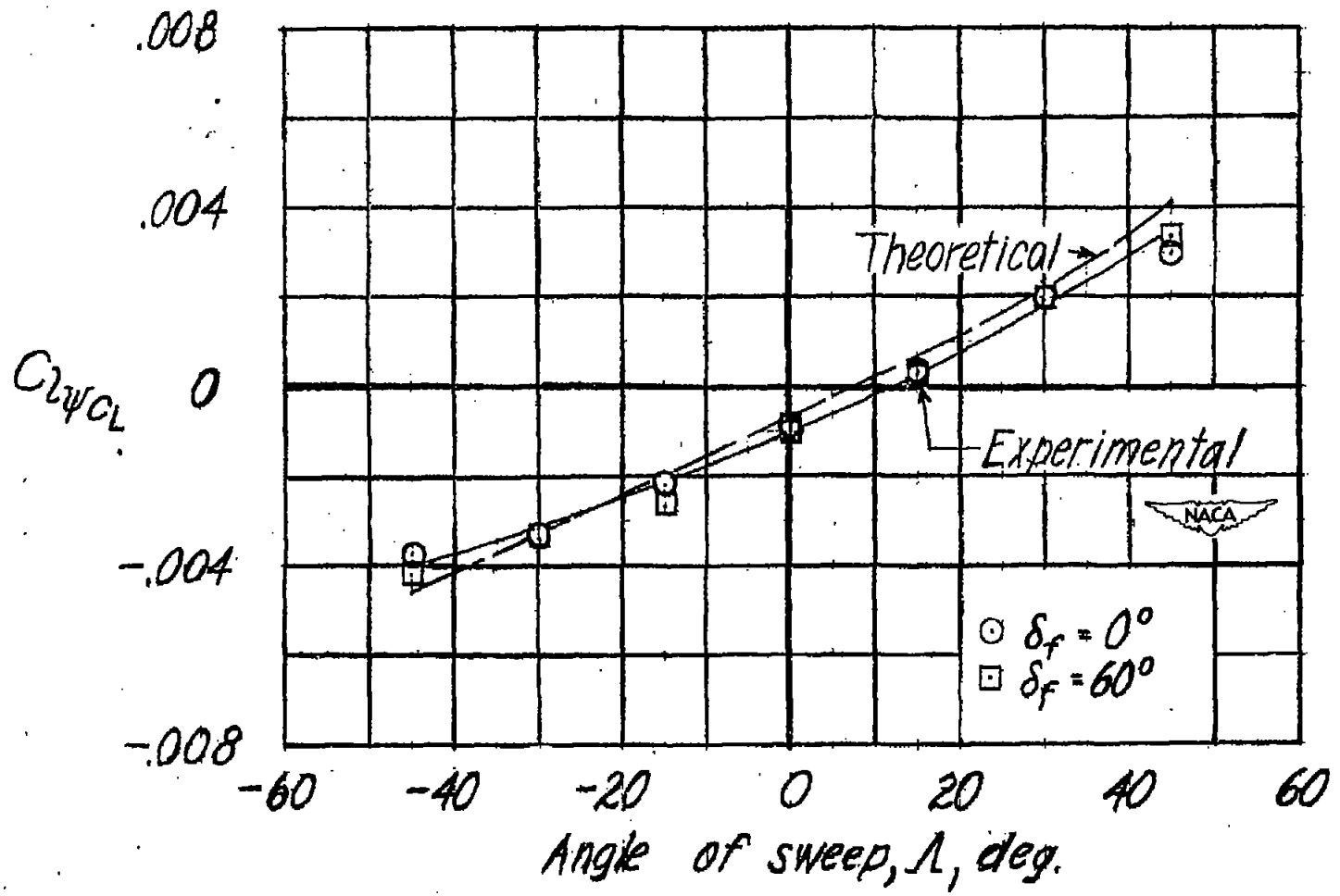

Figure 14.- Variation of $C_{l_{\psi C_L}}$ with sweep for models with various swept wings.

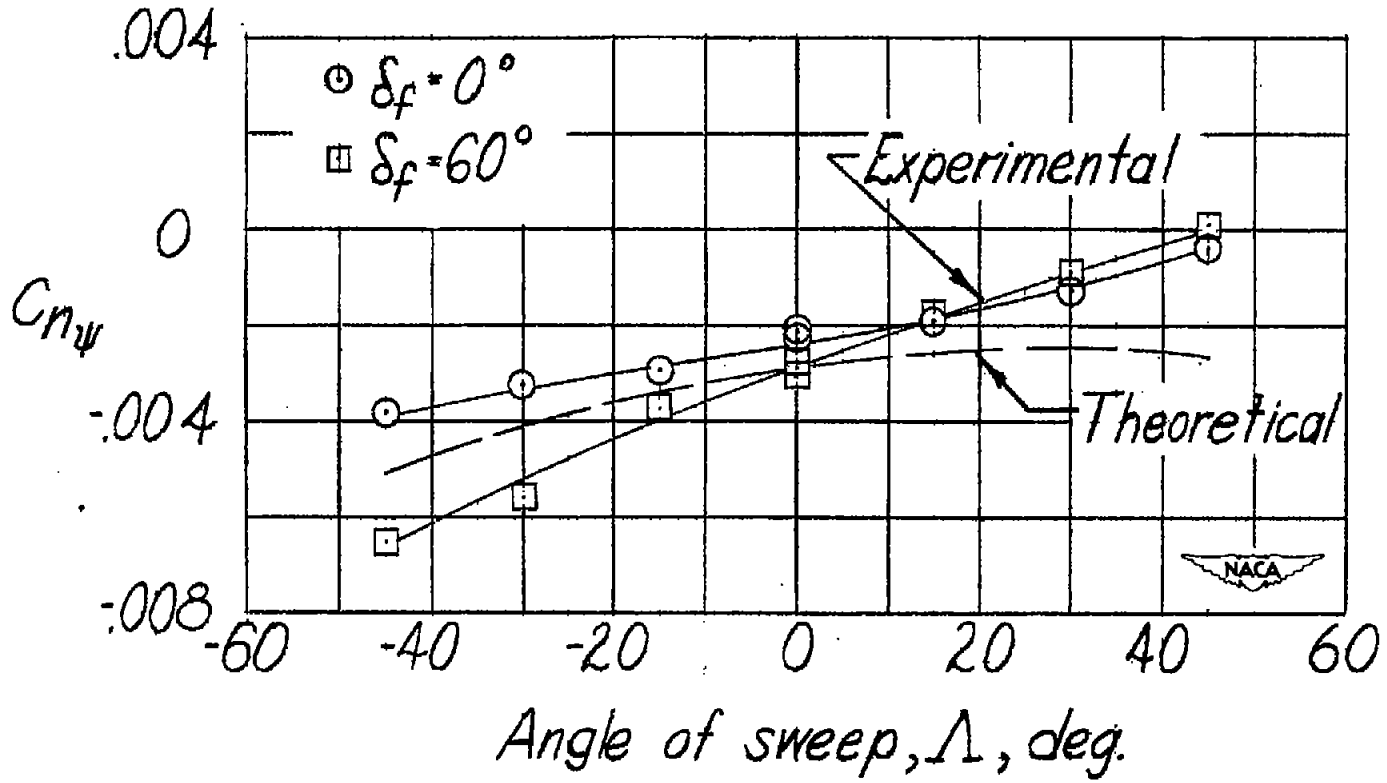

Figure 15.- Variation of C_{n_ψ} with sweep at zero lift for models with various swept wings.

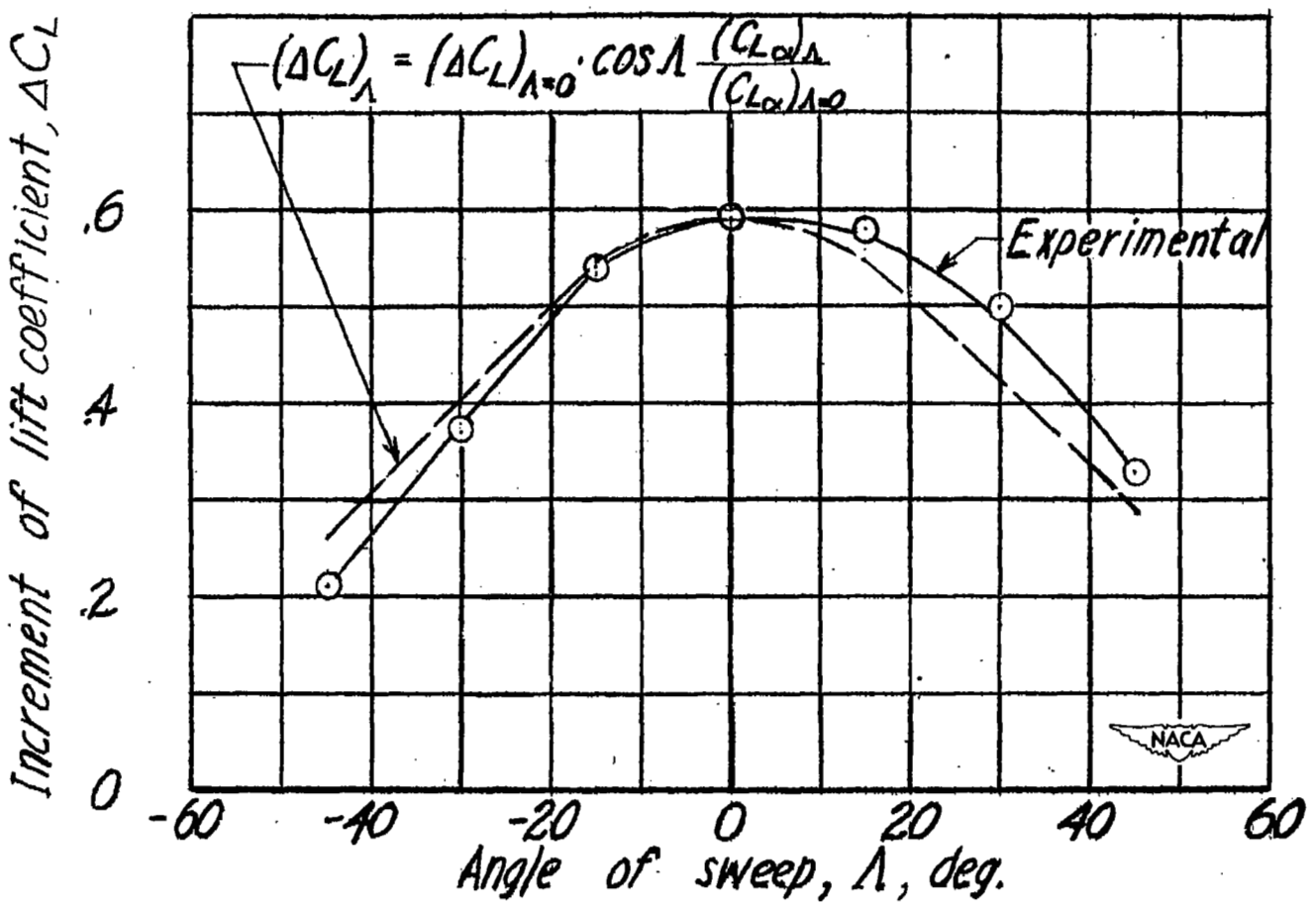

Figure 16.- Comparison between the theoretical and experimental effects of sweep on the increment of lift obtained at 0° angle of attack by deflecting the flaps 60°.